Marine Geology 326–328 (2012) 101–115

Contents lists available at SciVerse ScienceDirect
Marine Geology
journal homepage: www.elsevier.com/locate/margeo

Chemical weathering and provenance evolution of Holocene–Recent sediments from the Western Indus Shelf, Northern Arabian Sea inferred from physical and mineralogical properties

David R. Limmer [a,*], Cornelia M. Köhler [a], Stephen Hillier [b], Steven G. Moreton [c], Ali R. Tabrez [d], Peter D. Clift [e]

[a] School of Geosciences University of Aberdeen, Aberdeen, AB24 3UE, UK
[b] The James Hutton Institute, Craigiebuckler, Aberdeen, UK
[c] Natural Environment Research Council Radiocarbon Facility (Environment) East Kilbride, UK
[d] National Institute of Oceanography, Karachi, Pakistan
[e] Department of Geology and Geophysics, Louisiana State University, Baton Rouge, LA 70803, USA

ARTICLE INFO

Article history:
Received 15 December 2011
Received in revised form 14 July 2012
Accepted 17 July 2012
Available online 2 August 2012

Communicated by J.T. Wells

Keywords:
Indus Shelf
diffuse reflectance spectrophotometry
clay mineralogy
magnetic susceptibility

ABSTRACT

We present a multi-proxy mineral record based on X-ray diffraction and diffuse reflectance spectrophotometry analysis for two cores from the western Indus Shelf in order to reconstruct changing weathering intensities, sediment transport, and provenance variations since 13 ka. Core Indus-10 is located northwest of the Indus Canyon and exhibits fluctuations in smectite/(illite + chlorite) ratios that correlate with monsoon intensity. Higher smectite/(illite + chlorite) and lower illite crystallinity, normally associated with stronger weathering, peaked during the Early–Mid Holocene, the period of maximum summer monsoon. Hematite/goethite and magnetic susceptibility do not show clear co-variation, although they both increase at Indus-10 after 10 ka, as the monsoon weakened. At Indus-23, located on a clinoform just west of the canyon, hematite/goethite increased during a period of monsoon strengthening from 10 to 8 ka, consistent with increased seasonality and/or reworking of sediment deposited prior to or during the glacial maximum. After 2 ka terrigenous sediment accumulation rates in both cores increased together with redness and hematite/goethite, which we attribute to widespread cultivation of the floodplain triggering reworking, especially after 200 years ago. Over Holocene timescales sediment composition and mineralogy in two localities on the high-energy shelf were controlled by varying degrees of reworking, as well as climatically modulated chemical weathering.

1. Introduction

Understanding how climate change affects continental environments and weathering processes is a key component of quantifying solid Earth–climate interactions. Analysis of marine sediments holds out the prospect of being able to reconstruct this evolution over a number of timescales (e.g., Debrabant et al., 1993; Fagel et al., 1994; Colin et al., 1999; Abrajevitch et al., 2009). Geochemical analysis of Arabian Sea sediment has attracted significant interest from those seeking to reconstruct changing chemical weathering and provenance during the Cenozoic, over various timescales through analysis of elemental ratios or isotopic systems (e.g., Papavassiliou and Cosgrove, 1982; Suczek and Ingersoll, 1985; Fagel et al., 1994; Sirocko et al., 2000; Staubwasser and Sirocko, 2001; Clift and Blusztajn, 2005; Colin et al., 2006; Limmer et al., 2012). However, there has been limited interest in the physical and mineralogical properties of sediments in the Northern Arabian Sea over any timescale, especially during the Holocene to Recent, despite the relatively well-defined variability in climate and sea level known for this period. This lack of data is despite the fact that physical and mineralogical properties have been shown to be effective in tracing sediment transport in several areas worldwide (e.g., Balsam et al., 1995; Liu et al., 2003; Adler et al., 2009). The lack of a mineralogical record limits our ability to understand the impact that changing monsoon intensity has had on sediment composition sourced from a drainage basin with a strong erosional signal.

Mineralogy has been studied on the deep sea Indus Fan, but this has been starved of sediment since 11.5 ka (Prins et al., 2000) and contains no record spanning the Holocene, where we have the best climate records. Prior to 1947 under more natural conditions the Indus River delivered between 250 and 675 million tonnes of sediment to the Indus Delta annually (Milliman et al., 1984; Giosan et al., 2006) while since that time discharge has fallen sharply because of damming (Inam et al., 2007). However, it is possible that some anthropogenic impact on sediment flux occurred earlier starting with

* Corresponding author.
E-mail address: d.r.limmer@abdn.ac.uk (D.R. Limmer).

0025-3227
http://dx.doi.org/10.1016/j.margeo.2012.07.009

the agriculture of the Harappan Civilization, ~5 ka (Possehl, 1999). The Indus Shelf provides a potential archive for tracking changes in sediment discharge from the river and relating this to changing conditions in the onshore flood plain. The sediment record since the Last Glacial Maximum (LGM) is the target of this study reflecting the fact that this period has the best defined monsoon climate record derived from oceanographic upwelling records (Gupta et al., 2003), from speleothems (Fleitmann et al., 2003) and from lacustrine records in western India (Enzel et al., 1999).

The aim of this paper is to understand how evolving climate and sea level may have affected chemical weathering, as well sediment transport pathways and sources to the western shelf of the Indus delta (Fig. 1). We do this through examination of the physical properties and clay mineralogy of sediments deposited in that region. We focus on two Holocene–Recent cores taken from the Indus Shelf, which have already been the subject of a separate geochemical, weathering response and provenance study by Limmer et al. (2012). That study highlighted the importance of long-shore currents and the reworking of older sediment on the shelf, as well as direct supply from the Indus River in accounting for the sediment flux to the shelf during the Holocene. Applying a multi-proxy approach yields information about the transport, depositional history and origin of sediment on the Western Indus Shelf that cannot be obtained through analysis of individual sample methods. Moreover, application of continuous sensing methods allows rapid, cm-scale fluctuations to be examined in a way not possible with conventional geochemistry. The relative ease and low cost of sample preparation means a much larger and more complete dataset can be produced relatively quickly. We test the hypothesis that clay mineralogy, magnetic susceptibility and diffuse reflectance spectrophotometry can record changes in terrigenous sediment supply from the Indus River. We present a complete record of western Indus Shelf sedimentation based on whole core analysis and sampling. We use this record to investigate how sedimentation has changed in response to changes in monsoon strength and sea level.

2. Background

2.1. Regional setting

The Indus Shelf, located in the northern Arabian Sea spans approximately 180 km from the delta to the slope edge and stretches southeast from the Murray Ridge and Makran Coast to the Rann of Kutch in India (Fig. 1). The shelf is dominated by the submarine Indus delta and a large sinuous canyon structure, the Swatch (Giosan et al., 2006), separating the eastern and western shelves. The Holocene delta is built over an 11 km-thick passive margin sediment pile dating back to the Late Cretaceous and which has been the recipient of large volumes of sediment from the Indus River since at least the Early Miocene (Clift et al., 2001). The region is tectonically quiescent, except for the transform plate boundary to the west, along the Murray Ridge. Sediment supply is dominantly from the Himalayas and Karakoram (Clift et al., 2004; Garzanti et al., 2005).

Clay mineralogy and magnetic properties have been used to reconstruct palaeoenvironmental conditions and provenance of marine sediments throughout Asia (e.g., Bouquillon et al., 1989; Sirocko and

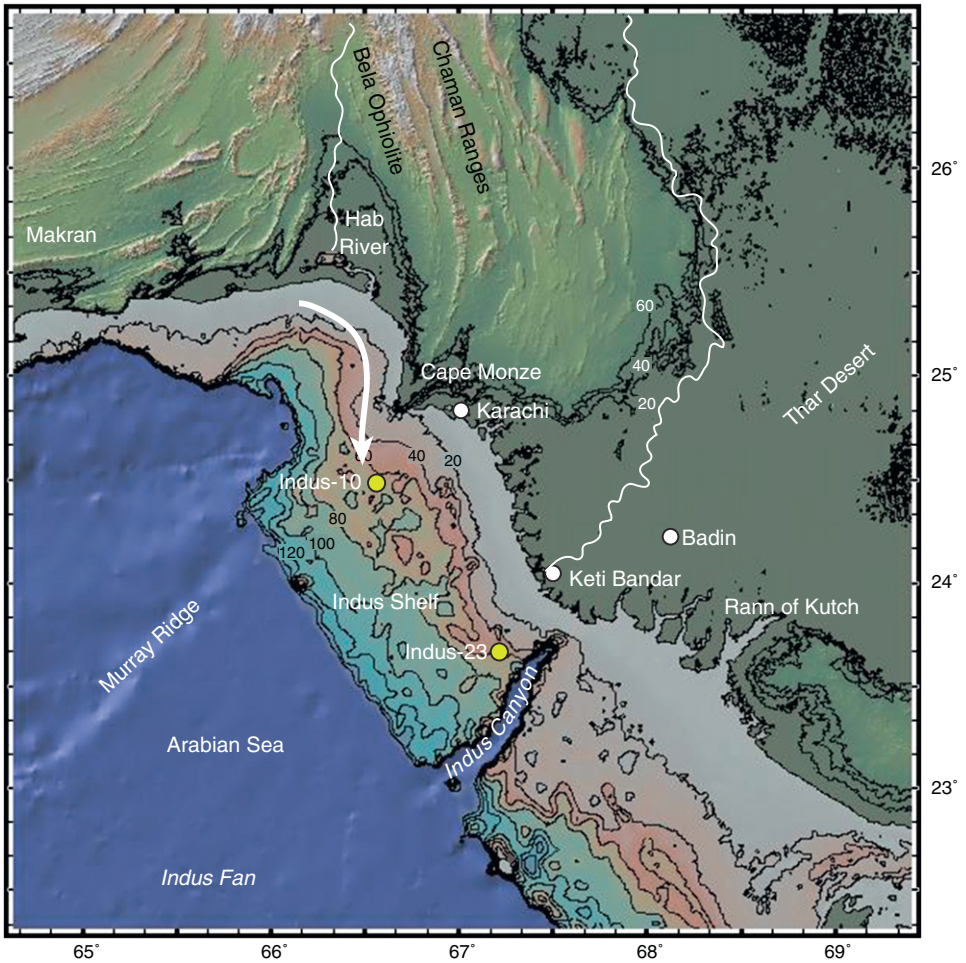

Fig. 1. Regional shaded bathymetry map of the northern Arabian Sea region adjacent to the Indus Delta showing onshore and offshore core sites, the Indus Canyon and Indus Fan. The white arrow shows the dominant direction of longshore current flow.

Lange, 1991; Prins et al., 2000; Thamban et al., 2002; Boulay et al., 2005; Wan et al., 2007; Liu et al., 2009). However, these studies have often been focussed in deepwater settings, away from the influence of major river systems or sediment processes on high-energy shelves. The cores in this study are located only 20 km away from the coast line in ~70 m of water, and are strongly influenced by the Indus River as well as the high wave energy of the Indus Shelf. As a result the two sites could potentially provide detailed records of Holocene environmental conditions recorded by the Indus River and delta system.

2.2. Clay mineralogy

Clay mineralogy has been widely used as a proxy for reconstructing climate, weathering and provenance in marine sediments. Changes in clay mineralogy have been linked to changes in weathering in the terrestrial environment of several Asian continental margins (e.g., Clift et al., 2002; Liu et al., 2003; Boulay et al., 2005; Wan et al., 2007; Colin et al., 2010) and as a record of terrestrial climate change in the deep Indian Ocean (Fagel et al., 1994). The major assumption made with palaeoclimatic interpretation of clay minerals is that there is no post-depositional diagenesis (Chamley, 1989; Hillier, 1995) which is likely to be true in a young, shallow-buried core such as we consider here. Typically studies quantify changes in the relative abundances of kaolinite, chlorite, smectite and illite as weathering proxies. In the Arabian Sea variations in clay mineralogy have been interpreted to reflect changes in the relative strength of dust plumes from Arabia, India and Pakistan, as well as changes in the input by major fluvial systems in the region (Sirocko and Lange, 1991; Fagel, 2007). Indus River assemblages are dominated by smectite, illite and to a lesser extent chlorite (Rao and Rao, 1995; Alizai et al., 2012).

Smectite is a product of chemical weathering and its presence is typically associated with alteration of volcanic minerals (Chamley, 1989; Liu et al., 2003), although it also forms in low-lying poorly-drained soils (Wilson, 1999). In contrast, kaolinite often forms in warm, wet tropical environments subject to strong leaching (Chamley, 2001; Thamban et al., 2002).

Both illite and chlorite can form through the breakdown of muscovite and biotite from or through the erosion of sedimentary rocks or minerals (Boulay et al., 2003). Chlorite and illite are usually preserved in soils and sediments at high-latitude or cooler climatic conditions where they are inherited from parent materials (Biscaye, 1965). Chemical weathering in these settings is weak but physical erosion is often stronger (e.g., Campbell and Claridge, 1982).

An additional property that has been used in clay mineral studies is the crystallinity index of illite, which is thought to be sensitive to alteration and thus to climate change (Chamley, 1989; de Visser and Chamley, 1990; Pandarinath, 2009). Low illite crystallinity is associated with greater chemical weathering (Pandarinath, 2009) or lower burial diagenesis (Kisch, 1983). High temperature and rainfall causes stronger weathering and thus wider XRD peaks and lower crystallinity. A stronger monsoon might favour greater hydrolyzation and stronger weathering causing a reduction in illite crystallinity (Lamy et al., 1998; Alizai et al., 2012).

2.3. Diffuse reflectance spectrophotometry (DRS)

DRS is applied to estimate mineral composition along a core using the reflectance of light (Balsam et al., 1999; St-Onge et al., 2007). The most simplistic and commonly used analysis of DRS data is that supplied by the Commission Internationale de l'Eclairage (CIE) (Debret et al., 2011) where the parameters L*, a* and b* are calculated (Balsam et al., 1999; Nederbragt et al., 2006; St-Onge et al., 2007). L*, often referred to as grey scale, represents lightness where 0 is dark and values of 100 are pale (Croft and Pye, 2004). L* has been widely used as a proxy for carbonate content (Rogerson et al., 2006). A* represents the red to green colour spectrum and is often used as an indicator of red mineral abundance, for example hematite (Croft and Pye, 2004; St-Onge et al., 2007). B* values represent the colour spectrum from yellow to blue (Croft and Pye, 2004; Almogi-Labin et al., 2009) and have been shown to respond to changes in organic matter (Debret et al., 2006; St-Onge et al., 2007). These values are calculated from the XYZ tri-stimulus coordinates (Rodgers et al., 2008). XYZ values are calculated from the material reflectance, the spectrum used and the standard observer values (Rodgers et al., 2008) and were also defined by the CIE (Croft and Pye, 2004). Because L* values have been shown to be affected by not only carbonate composition but also clay mineralogy (Balsam et al., 1999), we do not consider this to be suitable for this study.

Another use of DRS is to estimate the relative proportion of the iron-bearing minerals hematite and goethite. Increasing values of redness (a*) and hematite/goethite ratios have been shown to relate to drought phases because hematite forms under warm, arid conditions and goethite under cool, wet conditions (Schwertmann, 1971; Zang et al., 2007). Hematite/goethite ratios are often estimated using the first derivative peak of hematite, which occurs at 575 nm and the first derivative peak of goethite, which occurs at 565 nm (Helmke et al., 2002). A simplistic method is to divide the reflectance value at 565 nm by the reflectance value at 435 nm, which corresponds to peak reflectance of hematite and goethite.

2.4. Magnetic susceptibility

Magnetic susceptibility (χ) is a measure of magnetic mineral concentration (De Menocal et al., 1991). Magnetite, the main control of magnetic susceptibility, is associated with terrigenous sediment supply (Kumar et al., 2005). It is therefore possible to use magnetic susceptibility as a proxy for terrigenous sediment supply (De Menocal et al., 1991). It is widely used in a variety of marine and terrestrial settings as an indicator of changing environmental conditions and thus climate in the Asian monsoon region (e.g., De Menocal et al., 1991; Kumar et al., 2005; Thamban et al., 2005; Yancheva et al., 2007; Sun et al., 2009). It has been shown that increasing values of magnetic susceptibility correlate with periods of strengthening monsoon, as reconstructed from oxygen isotope records, revealing a link between Eolian transport and strong East Asian Winter Monsoon winds (An et al., 2001).

2.5. Records of Holocene monsoon evolution in Asia

A comprehensive review of climate records and the mechanisms for climate change are presented in Staubwasser and Weiss (2006). This section discusses periods of short-lived (500 years) changes in climate during the Holocene. Many authors have reported a trend for a period of strengthening of the SW Asian monsoon during the Early Holocene between ~10 ka and ~8 ka, followed by a gradual drying, especially between 6 and 2 ka (Enzel et al., 1999; Sarkar et al., 2000; Staubwasser et al., 2002; Fleitmann et al., 2003). Several periods of abrupt weakening of the SW Asian monsoon were identified by Gupta et al. (2003), using planktonic foraminifera at 8.2 ka, 6.2–5.8 ka, 4.6–4.2 ka, 3.2 ka and 2 ka–1.2 ka. These have since been linked short-lived solar minima events Gupta et al. (2005). It is this robust knowledge of climate history that allows us to use the clay mineral data presented here to understand the environmental response to the climate forcing.

3. Methodology

The techniques used to ascertain the mineralogy and physical properties of the sediment are magnetic susceptibility, DRS, X-ray diffraction (XRD), and bulk density porosity. XRD and DRS yield semi-quantitative data in the form of estimates of mineral composition. We use bulk

density with radiocarbon dating to calculate mass accumulation rates at the two core sites. The advantages of DRS and magnetic methods over bulk elemental and isotopic analyses are the relatively short sample preparation times and the speed of analysis. Apart from XRD all techniques are non-destructive and yield data for the entire core length.

We chose two cores obtained during the Winter 2008/09 aboard cruise 64PE300 of the RV *Pelagia* on the western shelf of the Indus Delta in the Arabian Sea (Fig. 1). Core Indus-10 is 9.06 m long was recovered from 71 m water depth and is located 120 km northwest of the modern Indus Canyon. Core Indus-23 is 7.67 m long and is located ~100 km southeast of Indus-10 in 70 m water depth (Fig. 1). Grain size variation is low, with mean grain size values ranging from 20 to 50 μm (Limmer et al., 2012). These provide excellent material for our chosen methods and also contained material suitable for ^{14}C AMS dating. Radiocarbon dating from these cores demonstrates these cores date back to the Early Holocene (Fig. 2) (Limmer et al., 2012). At Indus-10 there is a depositional hiatus approximately 830 cm below the present seafloor (cmbsf) (Fig. 3). A depositional hiatus near the base of the core is a transgressive surface, with Holocene material overlying sediments deposited during the Pleistocene and exposed during the last glacial, sea level lowstand. At Indus-23 a possible depositional hiatus in the Mid Holocene is identified at ~640 cmbsf below the present day seafloor (Fig. 4) (Limmer et al., 2012).

3.1. Clay mineralogy

Semi-quantitative clay mineralogy was conducted on 80 samples, 40 from each core. Each sample was placed in a beaker with 500 ml deionized water, sonicated with a probe for 5 min and stirred to disperse the material. Some samples were rinsed with deionised water several times to remove soluble salts and thereby aid dispersion. The dispersed sample was then transferred to a labelled, Atterberg cylinder topped up with deionized water, shaken and left for 16 h. The volume above a 20 cm sedimentation depth, which according to Stoke's law contains the <2 μm fraction was then syphoned into a labelled bottle. Specimens for XRD analysis were then made using the filter peel method (vacuum filtration) by transferring clay to a glass slide placed onto the filtrate, which was left to dry at room temperature (Hillier, 2003). The samples were run through a range of 2–45° 2θ on a Siemens D5000 X-Ray Diffractometer (XRD), with Co Kα radiation selected by a diffracted beam monochromator at The James Hutton Institute, Aberdeen, UK. Three diffraction patterns were recorded on the same specimen, air-dried, solvated in ethylene glycol by vapour pressure at 60 °C for 24 h and heating to 300 °C for 1 h (Hillier, 2003). Heating to 300 °C enhances the illite peak due to collapse of in any expandable clays such as smectite or mixed-layer illite–smectite (Moore and Reynolds, 1989; Hillier, 2003).

Analysis of the diffraction data was conducted by measuring peak intensity as peak area using Bruker Diffrac Plus EVA-12.0 software. Estimates of mineral composition were made by a reference intensity ratio method based on factors calculated with the Newmod programme as described in Hillier (2003). Illite crystallinity was measured using the full width at half maximum (FHWM) of the 001 basal illite peak and integral breadth (I Breadth) of the same peak (Kübler and Jaboyedoff, 2000). Both measurements are measured as values of Δ2°θ and show identical trends (Alizai et al., 2012). Because our cores are <9 m long, post-depositional burial diagenesis should not be a significant factor in clay mineral composition. Where clay mineral values are greater than 10% uncertainty is estimated as better than 5% weight at the 95% confidence level (Hillier, 2003). Clay mineral estimates are shown in Table 1.

3.2. Diffuse reflectance spectrophotometry (DRS)

Core scanning was conducted at the British Ocean Sediment Core Research Facility (BOSCORF) at the National Oceanography Centre, Southampton (NOCS) using a Geotek MSCL-XYZ with a Konica-Minolta CM2006d for spectrophotometry measurements. The archived halves were lightly scraped and carefully rewrapped in polyethylene to limit air bubble formation. Scanning was conducted at 1-cm resolution in order to generate a sufficiently high resolution record, while at the same time allowing for the collection of data in a reasonable duration. Wavelengths ranging from 360 nm to 740 nm at 10 nm intervals were recorded. This provided us with the full visible light spectrum, eliminating the problems of water absorption associated with greater wavelengths, while minimizing sample preparation (Jarrard and Vanden Berg, 2006). Values were measured as percentage reflectance compared to a barium sulphate calibration plate as a white standard (Balsam et al., 2000).

3.3. Magnetic susceptibility

Magnetic susceptibility values were measured on U-channels through all sections of Indus-10 and Indus-23 using a Barrington Instruments MS2 Magnetic Susceptibility metre at NOCS (Roberts and Lewin-Harris, 2000). Each U-channel was run three times and continuous measurements recorded every centimetre.

3.4. Bulk density

Data was collected using a Geotek MSCL-S at 1 cm resolution at NOCS. The cores were stored at room temperature the night before analysis and the data then processed using unpublished conductivity, temperature and depth (CTD) data obtained from the same cruise. We use bulk density in order to calculate mass accumulation rates (MAR) for both cores. MAR was calculated assuming linear sedimentation rates between dated samples and the bulk density values.

3.5. Age model

A total of 19 radiocarbon dates were obtained from the two core sites (Table 2), 15 of which were published in Limmer et al. (2012) using the marine standard calibration of Hughen et al. (2009). Analysis of the original 11 samples was completed at National Ocean

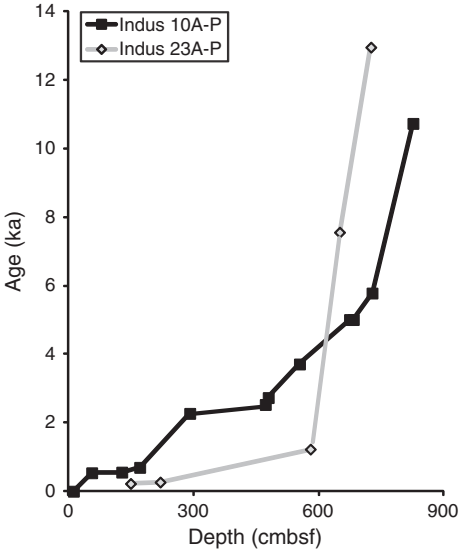

Fig. 2. Plot of age against depth based on ^{14}C ages from Limmer et al. (2012), showing increased sedimentation rates in the last 4 ky.

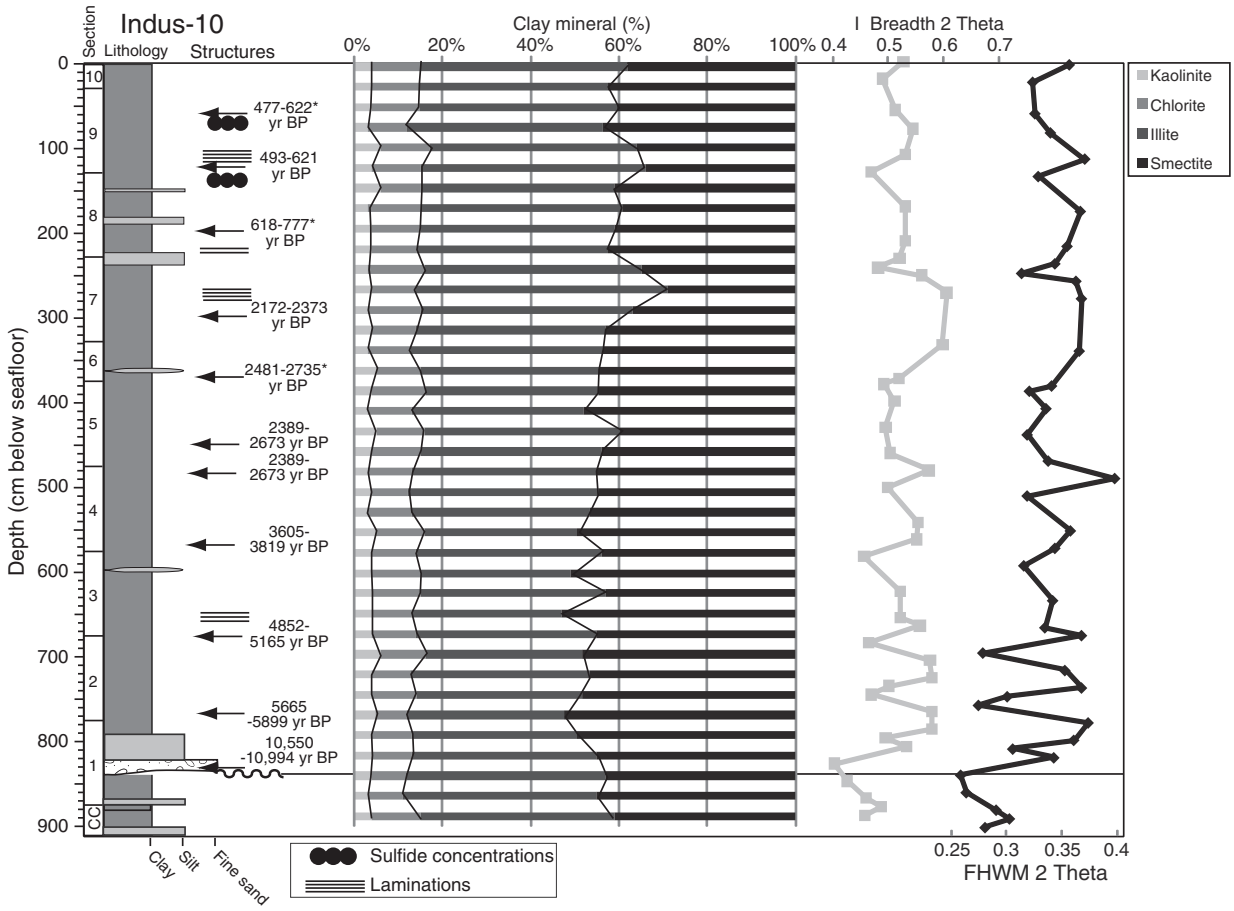

Fig. 3. Down-core variations in clay mineral abundances for Indus-10 showing a net decline in smectite and kaolinite above ~3.3 mbsf. Note also the significant variations in I-Breadth and FHWM between the core base and 680 cmbsf.

Sciences Accelerator Mass Spectrometry facility (NOSAMS, Woods Hole Oceanographic Institution, USA) using their standard method, as discussed by McNichol et al. (1995).

Four additional dates obtained from shell samples were prepared for radiocarbon analysis at the NERC Radiocarbon Facility (Environment) at East Kilbride, UK. Shells were ultrasonicated in deionized water and the outer 25% by weight of each shell was removed by controlled hydrolysis with dilute HCl. A known weight of homogenised, pre-treated shell was hydrolysed to CO_2 using 85% orthophosphoric acid at room temperature. The resulting CO_2 was cryogenically trapped and a subsample of CO_2 was collected for independent $\delta^{13}C$ measurement. The remaining CO_2 was converted to graphite by Fe/Zn reduction. The $\delta^{13}C$ value was measured on a dual inlet stable isotope mass spectrometer (VG OPTIMA) and is representative of $\delta^{13}C$ in the original, pre-treated sample material (quoted precision is the machine error). Graphite targets were analysed at the AMS Laboratory, East Kilbride and the results were corrected to $\delta^{13}C$ Vienna Pee Dee Belemnite standard (VPDB‰ −25) using the $\delta^{13}C$ values.

For this study all ages were remodelled using Calib 6.0 calibration software (Hughen et al., 2009) and the Marine09 dataset (Reimer et al., 2009). A local marine reservoir correction (ΔR) of +232 ± 26 years was used based on the average reservoir age of two samples from a similar location to the Indus core sites, as shown on the 14Chrono Marine Reservoir Database (http://calib.qub.ac.uk/marine/). We note that two samples, one at Indus-10 (373 cmbsf) and one at Indus-23 (578 cmbsf) do not fit the general age model. In both cases these shells were unarticulated and located close to sandier sections of the cores implying that they could be reworked. They are not included in calculating sedimentation rates or the age model (Fig. 2). All the dated samples are included in Table 2 with the new ages highlighted in bold.

4. Results

4.1. Clay mineralogy

The relative abundances of four minerals smectite, illite, chlorite and kaolinite were plotted together with the illite crystallinity proxies of I Breadth and FHWM for Indus-10 (Fig. 3). Beneath the depositional hiatus illite is slightly more abundant than smectite, with values of 44% for illite compared to values of 41% for smectite. Above the depositional hiatus, between 480 cmbsf and 760 cmbsf, smectite is generally the more abundant mineral, although the change is very modest. Smectite values range from 44 to 53%, while illite values range from 34 to 43%. Above 480 cmbsf illite is generally more abundant than smectite (39–51% compared to 38–44%). Both minerals are far more abundant than kaolinite (3–6%) and chlorite (7–12%). The illite crystallinity proxies both show sharp increases above the depositional hiatus between 760 cmbsf and 835 cmbsf from 0.26 to 0.37 FHWM Δ2°θ and 0.40 to 0.57 I-Breadth Δ2°θ (i.e. lower crystallinity). Above 480 cmbsf illite crystallinity remains low apart from two declines in FHWM Δ2°θ from 0.40 to 0.31 and in I-Breadth Δ2°θ from 0.60 to 0.48 at 240 cmbsf. There is also a slight increase in crystallinity at 130 cmbsf where FHWM Δ2°θ drops from 0.36 to 0.33 and I-Breadth Δ2°θ from 0.53 to 0.47.

At Indus-23 (Fig. 3) illite crystallinity values remain very stable throughout the core with values that are generally lower (i.e., more crystalline, less altered) than those observed in Indus-10. FHWM

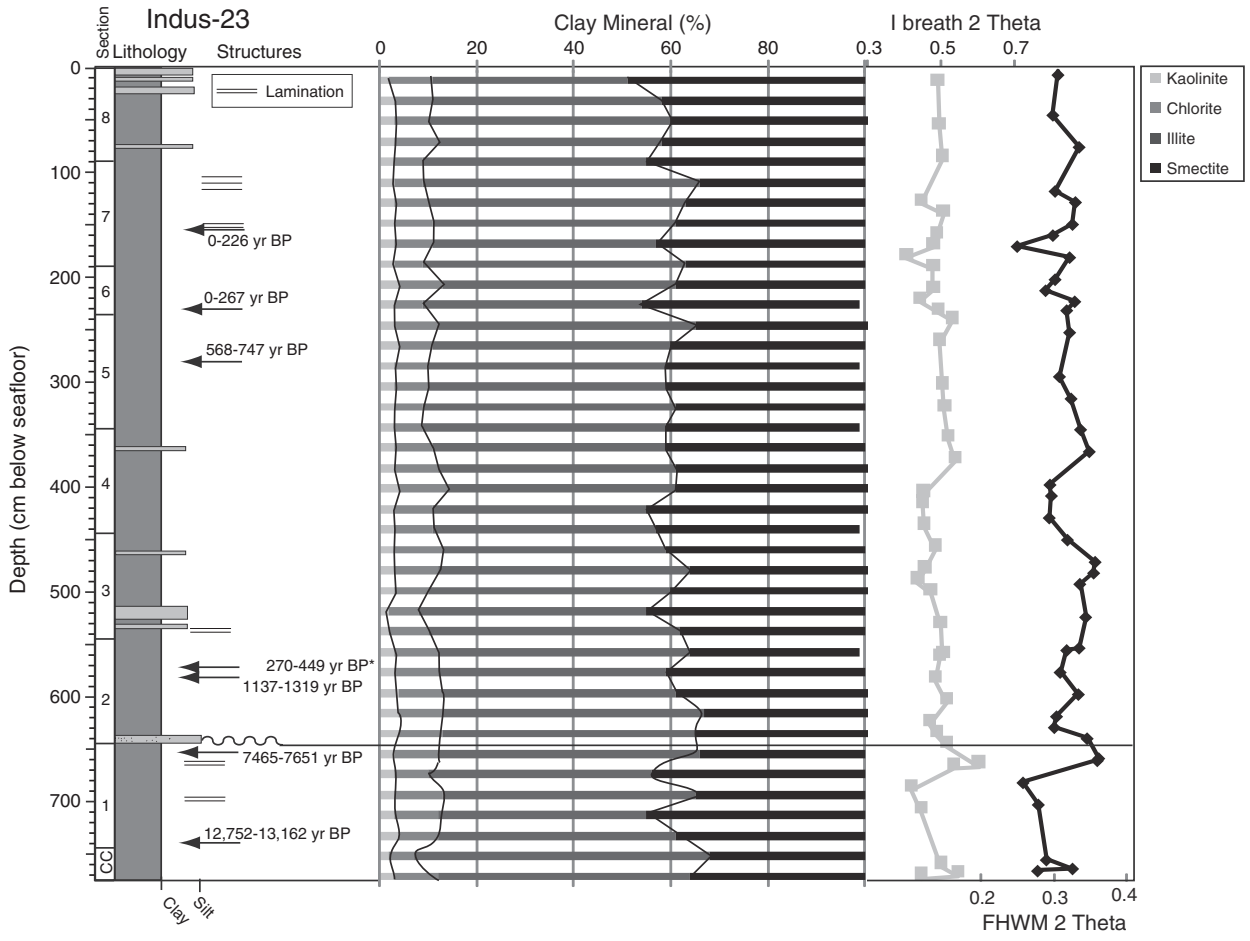

Fig. 4. Down-core variations in clay mineral ratios for Indus-23. There is an increase in illite crystallinity below 680 cmbsf, but generally the clay mineral assemblage is remarkably consistent through the length of the core.

Δ2°θ ranges 0.33–0.36 and I-Breadth Δ2°θ 0.45–0.53 at Indus-23. Illite (46–52%) seems more dominant than smectite (35–45%) throughout Indus-23. Smectite and illite are the dominant mineral groups, although chlorite contents do increase (from ~7 to 11%) when smectite values generally decline (~53 to 36%) in both cores.

4.2. Magnetic susceptibility, DRS and bulk density

Magnetic susceptibility, redness, hematite/goethite ratios and bulk density values were plotted with the sedimentary log for Indus-10 (Fig. 5). There is no clear correlation between sediment type and any of these geophysical proxies, apart from at the depositional hiatuses. Four areas where variations in patterns shift sharply are highlighted. Above the depositional hiatus at ~850 cmbsf magnetic susceptibility increases from 75×10^{-6} SI to approximately 260×10^{-6} SI at 700 cmbsf, while redness and hematite/goethite ratios values decline sharply from ~2.8% to 0.8% and 1.8 to 0.8 respectively. At 550 cmbsf magnetic susceptibility, redness and hematite/goethite values all increase sharply while bulk density values decrease. Similar shifts also occur at ~440 cmbsf and at ~220 cmbsf respectively.

Magnetic susceptibility, redness, hematite/goethite and bulk density variations were plotted with the sedimentary log for Indus-23 (Fig. 6). As at Indus-10 lithology does not appear to be a key control on proxy values, not least because there is not much lithological variation. Magnetic susceptibility values decline sharply at 680 cmbsf from 300×10^{-6} SI to almost zero before rebounding back and reaching values 380×10^{-6} SI at 660 cmbsf across the depositional hiatus. At the same point redness values initially decreases from ~1.3% to ~0.4% to close to zero at 660 cmbsf. At ~640 cmbsf magnetic susceptibility values increase, redness and hematite/goethite values peak at 2.2% and 1.9. Similar patterns are observed at 350 cmbsf.

4.3. Temporal variations in clay mineralogy

Clay mineral ratios are calculated with the chemical weathered clays (smectite and kaolinite) divided by the physically eroded clay minerals (chlorite and illite) in order to generate a proxy for the relative intensity of chemical weathering although kaolinite-based values are of doubtful value because of the generally low concentrations of this mineral. Values for smectite/illite and smectite/(chlorite + illite) are generally lower in Indus-23 than Indus-10 (Fig. 7). We employ smectite/(chlorite + illite) because it has already been demonstrated to be effective in similar Quaternary sediments from the Mekong Delta (Colin et al., 2010). However, the smectite/chlorite value is generally higher in Indus-23 than in Indus-10. Below the hiatus in Indus-23 (~7.5 ka), both cores show very similar patterns in clay mineralogy, although there is an increase in all ratios in Indus-10 between 13 ka and 9 ka. In Indus-10 all smectite-based ratios increase to very high values (e.g., 1.2 for smectite/illite and 1.1 for smectite/(chlorite + illite)) after ~2.5 ka before declining sharply at 2 ka (e.g., 0.4 for both smectite/illite and smectite/(chlorite + illite)). Smectite/(chlorite + illite) again increase to 0.8 after ~0.5 ka (Fig. 8).

A much higher resolution record is available for the last 1.5 ka from core Indus-23 (Fig. 8). A net increase in smectite/illite (0.7 to 1.3), smectite/(chlorite + illite) (0.5 to 1.0) and smectite/chlorite (4 to 6) is observed. Much of this change appears to have happened in

Table 1
Abundance estimates for clay minerals for both Indus-10 and Indus-23 based on analysis of X-ray diffraction data.

Sample	Age (yr BP)	Depth (cmbsf)	Kaolinite (%)	Chlorite (%)	Illite (%)	Smectite (%)	FHWM 2 theta	I Breadth 2 theta
10AP10-0	231	0	4	11	47	38	0.36	0.53
10AP10-20	308	20	4	11	43	43	0.32	0.49
10AP9-28	550	56	4	11	45	41	0.33	0.51
10AP9-40	552	78	3	9	45	44	0.34	0.55
10AP9-80	555	108	6	11	47	36	0.37	0.53
10AP8-0	557	128	4	11	51	34	0.33	0.47
10AP8-40	688	168	6	9	44	41	0.37	0.53
10AP8-80	1182	208	3	12	45	39	0.36	0.53
10AP7-0	1445	228	4	11	44	41	0.34	0.52
10AP7-31	1590	239	4	10	43	42	0.31	0.48
10AP7-40	1708	248	3	13	49	35	0.36	0.56
10AP6-0	2325	328	3	12	48	37	0.37	0.60
10AP6-40	2382	368	4	10	43	43	0.34	0.52
10AP5-0	2391	374	3	10	44	44	0.32	0.49
10AP5-20	2420	394	5	10	40	44	0.34	0.51
10AP5-50	2462	424	4	12	39	44	0.32	0.50
10AP4-0	2560	474	5	11	44	40	0.40	0.57
10P4-20	2853	494	4	11	41	44	0.32	0.50
10AP4-60	3438	534	3	10	42	45	0.36	0.56
10AP4-80	3712	554	4	8	43	44	0.34	0.55
10AP3-0	3928	574	3	10	40	46	0.32	0.46
10AP3-40	4360	614	5	11	35	50	0.34	0.52
10AP3-71	4695	645	4	10	42	44	0.34	0.52
10AP3-80	4792	654	4	11	34	51	0.37	0.56
10AP2-0	5009	674	4	11	42	43	0.28	0.47
10AP2-20	5295	694	4	9	34	53	0.35	0.58
10AP2-40	5581	714	4	10	41	45	0.37	0.58
10AP2-60	6085	734	4	10	41	44	0.28	0.47
10AP2-80	7095	754	6	10	35	48	0.37	0.58
10AP1-0	8105	774	4	9	41	47	0.36	0.58
10AP1-10	8611	784	4	10	37	48	0.31	0.50
10AP1-20	9116	794	5	7	36	53	0.34	0.53
10AP1-40	10,126	814	4	9	37	49	0.26	0.40
10AP1-60	11,370	834	4	9	42	45	0.26	0.43
10AP1-80	20,000	854	4	8	45	43	0.29	0.46
10AP1-90	20,000	864	3	8	44	45	0.30	0.49
10APCC-0	20,000	874	4	11	44	41	0.28	0.46
23AP8-20	15	20	2	9	40	49	0.32	0.49
23AP8-60	46	60	3	8	47	42	0.33	0.49
23AP7-0	67	89	3	7	50	41	0.36	0.50
23AP7-30	98	129	3	9	46	42	0.33	0.45
23AP7-40	105	139	3	6	46	45	0.36	0.52
23AP7-60	113	149	3	6	57	34	0.35	0.50
23AP7-70	116	159	3	7	53	37	0.33	0.49
23AP7-80	119	169	3	8	50	39	0.28	0.41
23AP6-0	125	189	3	8	46	43	0.35	0.50
23AP6-20	130	209	3	6	54	37	0.33	0.48
23AP6-30	133	219	4	9	48	39	0.32	0.49
23AP6-40	161	229	3	6	45	45	0.34	0.49
23AP5-0	186	237	3	9	53	36	0.34	0.53
23AP5-20	248	257	4	7	49	40	0.35	0.50
23AP5-60	372	297	3	7	49	40	0.33	0.50
23AP5-80	434	317	3	7	49	41	0.35	0.51
23AP4-0	521	345	3	6	52	39	0.37	0.54
23AP4-20	583	365	3	6	50	40	0.38	0.54
23AP4-50	676	395	3	8	48	41	0.32	0.45
23AP4-60	707	405	3	9	49	42	0.33	0.47
23AP4-80	769	425	4	10	47	40	0.32	0.45
23AP3-0	831	445	3	8	44	46	0.35	0.49
23AP3-20	893	465	3	8	46	42	0.34	0.47
23AP3-30	924	475	3	10	46	41	0.34	0.46
23AP3-40	955	485	3	9	52	42	0.34	0.48
23AP3-70	1048	515	3	7	50	45	0.35	0.49
23AP3-98	1135	543	2	6	47	45	0.36	0.51
23AP2-0	1141	545	2	8	52	38	0.35	0.50
23AP2-20	1203	565	3	9	52	35	0.34	0.48
23AP2-40	1258	585	3	9	47	41	0.36	0.52
23AP2-60	1307	605	4	9	48	40	0.33	0.47
23AP2-70	1331	615	4	9	54	34	0.33	0.49
23AP2-80	1356	625	4	9	52	36	0.37	0.52
23AP2-100	6983	643	3	9	54	34	0.39	0.54
23AP1-0	7463	645	3	7	46	44	0.39	0.60
23AP1-20	8638	665	3	10	52	35	0.28	0.42

(continued on next page)

Table 1 (*continued*)

Sample	Age (yr BP)	Depth (cmbsf)	Kaolinite (%)	Chlorite (%)	Illite (%)	Smectite (%)	FHWM 2 theta	I Breadth 2 theta
23AP1-40	10,078	685	3	9	43	45	0.31	0.47
23AP1-90	13,000	735	4	8	49	39	0.32	0.50
23AP1-100	13,100	743	2	5	61	32	0.35	0.55
23APCC-0	13,200	745	3	9	52	36	0.30	0.45

the past 200 years. An opposing trend is observed in kaolinite/illite. The smectite/kaolinite ratio follows the pattern of smectite-based ratios (e.g., smectite/chlorite). In contrast, the Indus-10 record for the last 1.5 kyr shows a significant scatter in all clay mineral ratios at ~0.6 ka that is not observed at Indus-23, while the kaolinite/illite increases between 1.2 ka and 0.6 ka.

5. Discussion

The variations in clay mineralogy at both core sites are consistent with previously published data for the Arabian Sea (Sirocko and Lange, 1991) and Indus Fan (Kolla et al., 1981) in that smectite and illite are the dominant mineral groups. The data from Indus-10 and Indus-23 agree with recent work from the onshore delta and floodplains where chlorite was observed to account for less than 10% of the total clay assemblage (Alizai et al., 2012). Consistently low kaolinite values of 3–5% are also consistent with previously published work in the region that show that kaolinite concentrations are generally the highest in the central Arabian Sea (Sirocko and Lange, 1991).

In order to compare our clay mineral assemblages with those from the onshore (Alizai et al., 2012), a ternary plot of kaolinite, smectite and (chlorite + illite) was constructed (Fig. 9). This plot shows that both the river mouth site at Keti Bandar and Indus-10, located in the northwest of the study area have very similar clay compositions. However, sediments from Indus-23 have consistently higher smectite contents. This indicates that sediment deposited at Indus-23 was eroded from a source that is generally more chemically weathered than that deposited at the river mouth. Such a source could include older sediments deposited before the Holocene, or that this part of the shelf was receiving sediment from a region where more smectite-producing rocks are exposed. Indeed the contrast between Indus-23 and the river mouth is quite surprising given their close proximity.

Table 2
Full list of samples dated by AMS radiocarbon dating, including unpublished ages in bold.
Modified from Limmer et al. (2012).

Type	Sample	Depth (cmbsf)	Age (yr BP)	Age uncertainty (yr)	Calibrated Age 2 sigma (yr BP)
Mollusc	10AP10,12 cm	12	630	15	N/A
Mollusc	**10AP9, 28 cm**	**56**	**1166**	**35**	**477–549**
Mollusc	10AP9, 98 cm	128	1180	25	493–621
Mollusc	**10AP8, 43 cm**	**171**	**1365**	**35**	**618–777**
Mollusc	10AP7, 63 cm	291	2850	15	2172–2373
Mollusc	**10AP6, 45 cm**	**373**	**3099**	**35**	**2481–2735**
Mollusc	10AP5, 98 cm	472	3020	15	2389–2673
Mollusc	10AP4, 7 cm	479	3020	15	2789–2673
Mollusc	10AP4, 80 cm	554	4000	20	3605–3819
Mollusc	10AP3, 98 cm	674	4980	20	4852–5164
Mollusc	10AP2, 9 cm	683	4980	20	4852–5165
Mollusc	10AP2, 54 cm	728	5650	40	5665–5899
Mollusc	10AP1,52 cm	826	10,050	45	10,550–10,914
Mollusc	23AP7, 60 cm	149	695	25	0–226
Mollusc	23AP6, 31 cm	220	765	30	0–267
Mollusc	23AP2, 28 cm	580	1910	35	1137–1319
Mollusc	**23AP2, 35 cm**	**587**	**939**	**35**	**450–270**
Mollusc	23AP1, 5 cm	650	7310	40	7465–7651
Mollusc	23AP1, 80 cm	725	11,750	60	12,752–13,162

5.1. Clay mineralogy as provenance tool: comparing onshore to offshore

Clay mineralogy is known to be related to provenance in dust samples within the Arabian Sea. In order to assess whether clay mineralogy relates to provenance in this setting we compared the smectite/(chlorite + illite), smectite/kaolinite and kaolinite/illite with the neodymium isotope characteristics of the sediments because this isotope system is widely accepted as a reliable provenance proxy that is not affected significantly by chemical weathering (Goldstein et al., 1984) (Fig. 10). We exploit bulk neodymium isotope (as expressed by ε_{Nd}) data from these same cores published by Limmer et al. (2012) and from the coast at Keti Bandar, where sedimentation is believed to track sediment delivery at the river mouth (Clift et al., 2008). Neodymium isotopes are known to be sensitive to source changes in the Indus basin (Clift et al., 2002). In both offshore cores less negative ε_{Nd} (i.e., less continental, less Himalayan) is often, but not always, associated with higher smectite/(chlorite + illite) ratios. However, more negative ε_{Nd} values are associated with a range of smectite/(chlorite + illite) ratios (Fig. 10A) and the highest smectite/(chlorite + illite) values are never associated with the least negative ε_{Nd} values. The kaolinite/illite ratio (Fig. 10B) is associated with a range of ε_{Nd} values, both onshore and offshore. Overall there is no correlation between clay mineralogy and ε_{Nd}.

We further compare the temporal evolution in neodymium isotope values with the variation in clay mineralogy in the two cores considered here, as well as from the river mouth (Alizai et al., 2012) (Fig. 11). Since ~11 ka the two core sites show less negative ε_{Nd} values compared to sediment deposited near the river mouth at Keti Bandar, although the discrepancy is most pronounced at Indus-10. This difference indicates that the sediment at the core sites is not totally dominated by direct flux from the Indus River at any given time. Indus-10 has received sediment from the Bela Ophiolite the west of the study area via longshore drift during the Early Holocene (Limmer et al., 2012), although the clay mineralogy does not reflect this change. The one ε_{Nd} value from Indus-23 during the Early Holocene suggests that the sediment had more in common with Indus River sediment from the LGM rather than the active river, a hypothesis that is consistent with the less weathered state of the material. Together these data may indicate reworking of sediments on the shelf, for example those deposited and exposed during the LGM. In general however, the smectite/(chlorite + illite) ratios of the Indus sediments show higher values (more weathering) between 10 and 5 ka, when the monsoon was stronger. As the climate dried falling smectite/(chlorite + illite) ratios are consistent with the notion of less chemical weathering, and supportive of a dominant flux from the Indus River to the core sites. The shift towards less negative ε_{Nd} values in Indus-10 at ~3 ka is probably linked to reworking of older shelf sediments (Limmer et al., 2012). During the recent past, especially the last 200 years the overall pattern both in the on and offshore record is a net increase in the smectite/(chlorite + illite) ratios, following a period of falling ratios between 6 and 2 ka at Indus-10 and a shift towards more negative ε_{Nd} values. This more recent change is unlikely to be linked to natural climate changes but coincides with the onset of large scale agriculture across the Indus basin.

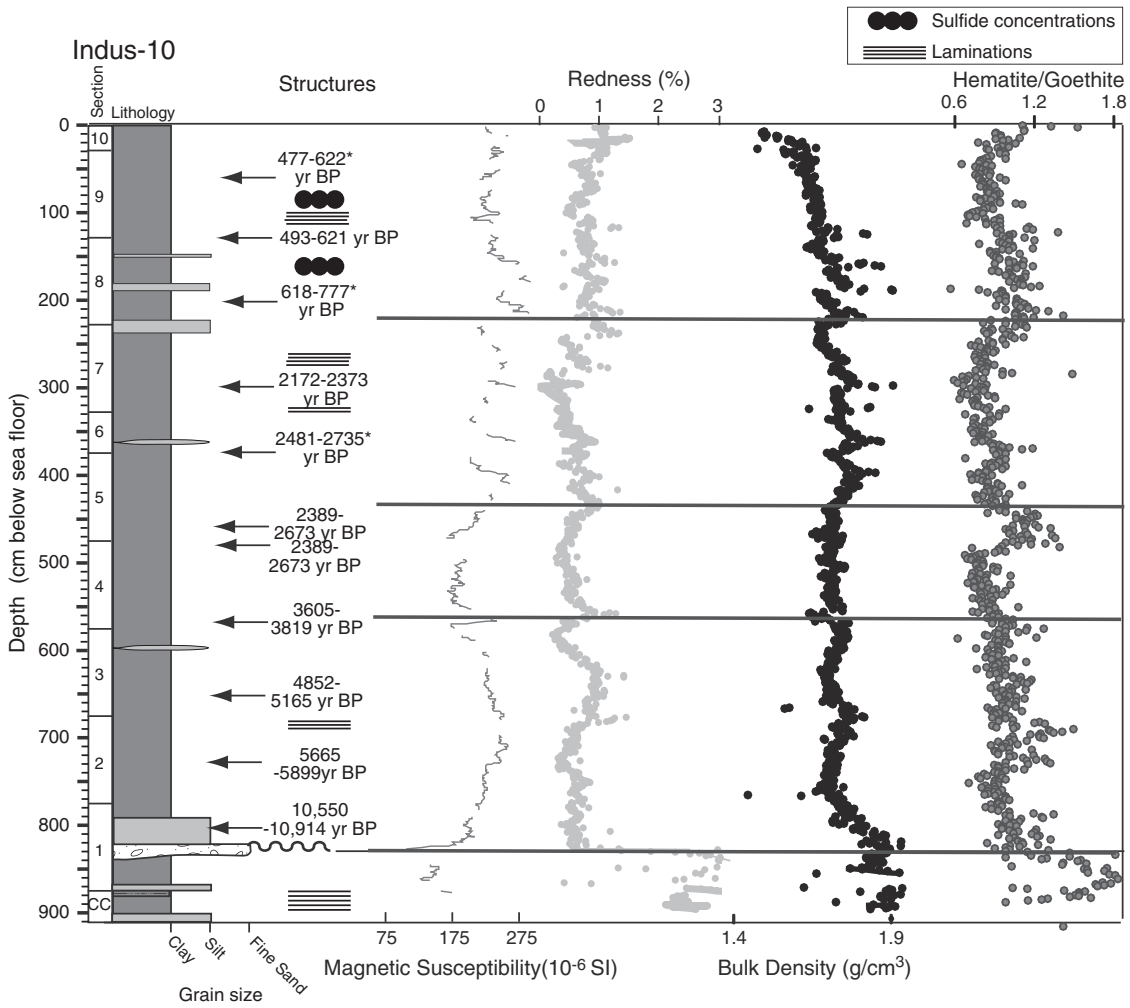

Fig. 5. Down-core variation in magnetic susceptibility, redness, hematite/goethite and bulk density from Indus-10. Redness and hematite/goethite values drop sharply above the depositional hiatus but also peak at ~450 cmbsf.

5.2. Clay mineralogy as a weathering proxy

Because of their contrasting origins kaolinite/illite ratios have been used as proxies for hydrolysis compared to physical erosion intensity in marine sediments (Chamley, 1989). Kaolinite/illite has also been used as a proxy for humidity (Thamban et al., 2002). Another commonly used ratio is smectite/(chlorite + illite), which is interpreted to reflect the proportion of chemically weathered material compared to physically weathered material (e.g., Boulay et al., 2005; Alizai et al., 2012). As a result, this ratio is a useful weathering indicator in sub-tropical and arid environments where there is little kaolinite present.

Figs. 7 and 8 plotted clay minerals associated with chemical weathering against clay minerals associated with physical weathering over time in order to determine how intensity has changed with time. If greater values of kaolinite and smectite reflect increased chemical weathering then smectite/illite and kaolinite/illite would show identical patterns through time, which is not the case. This is because smectite is favoured by drier, more seasonal conditions, while kaolinite is formed by leaching in wet, tropical environments (Thiry, 2000). We further test the ability of clay minerals to act as weathering proxies by comparing them with K/Al, which is the weathering proxy that is least affected by grain size or carbonate content, at least on the Indus Shelf (Limmer et al., 2012) (Fig. 12). For all three clay mineral ratios there is a poorly defined negative relationship between weathering intensity from the geochemistry and the weathering intensity in the clay mineralogy, although some of this relationship may be caused by the effects of grain size, this could also be attributed to the loss of potassium and the increase in both kaolinite and smectite during chemical weathering. Such proxies need to be used with some care because K is enriched under moderate degrees of chemical weathering, but then becomes depleted under more intense weathering, as K-feldspars break down (Blaxland, 1974; Nesbitt et al., 1997). We suggest that the anti-correlation noted in Fig. 12C in particular reflects the relatively moderate degree of alteration in Indus River sediments. The generally higher values for smectite relative to illite in Indus-10 could also reflect the mixing of Bela Ophiolite-derived sediments into Indus-10 rather than increased chemical weathering.

5.3. Response to Holocene sea level rise and monsoon intensification

Temporal variations in magnetic susceptibility, mass accumulation rates, clay mineralogy, redness, illite crystallinity (FHWM) and hematite/goethite ratios are plotted against the Qunf Cave climate record of Fleitmann et al. (2003) (Fig. 13). The clay mineral proxy smectite/(chlorite + illite), as well as illite crystallinity, shows clearly that strong monsoons are associated with periods of more intense weathering. A similar coherent relationship between smectite/(chlorite + illite) and monsoon strength has been observed elsewhere in Asia (Colin et al., 1999). Interestingly, the start of the period of stronger weathering between 11 and 8 ka is also a time when hematite/goethite and redness increased. Normally these trends would be associated with drier rather

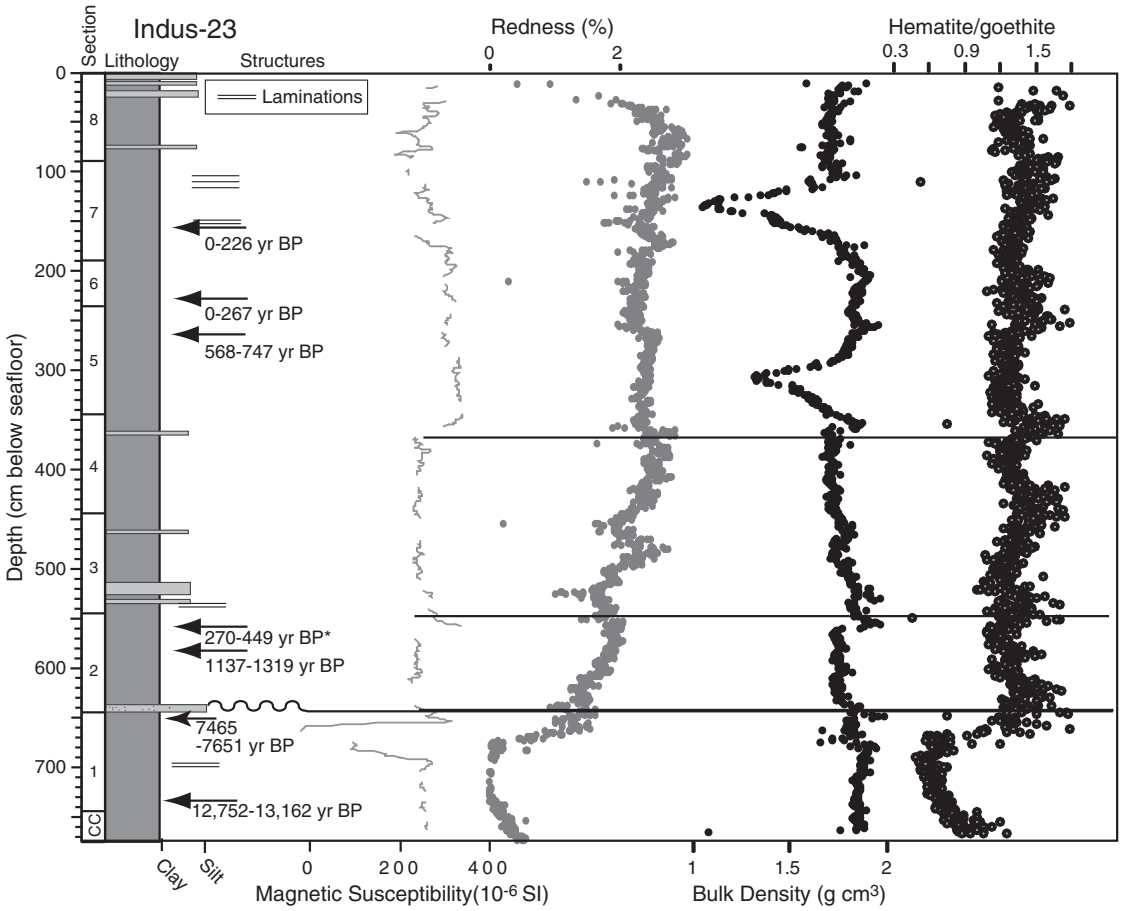

Fig. 6. Down-core variation in magnetic susceptibility, redness, hematite/goethite and bulk density from Indus-23. Results show a major spike in magnetic susceptibility, a net increase in redness and hematite/goethite across the depositional hiatus at ~650 cmbsf.

than wetter conditions, yet are superior climate record clearly rules this out in this case. We suggest that the change in hematite/goethite reflects erosion and reworking of pre-existing hematite-rich soils formed during the arid LGM period and our reworked during the period of intensifying monsoon in the Early Holocene. Alternatively, the high hematite abundance may be associated with increased seasonality (i.e. monsoonal conditions) (Schwertmann, 1971; Ji et al., 2005; Naidu, 2006).

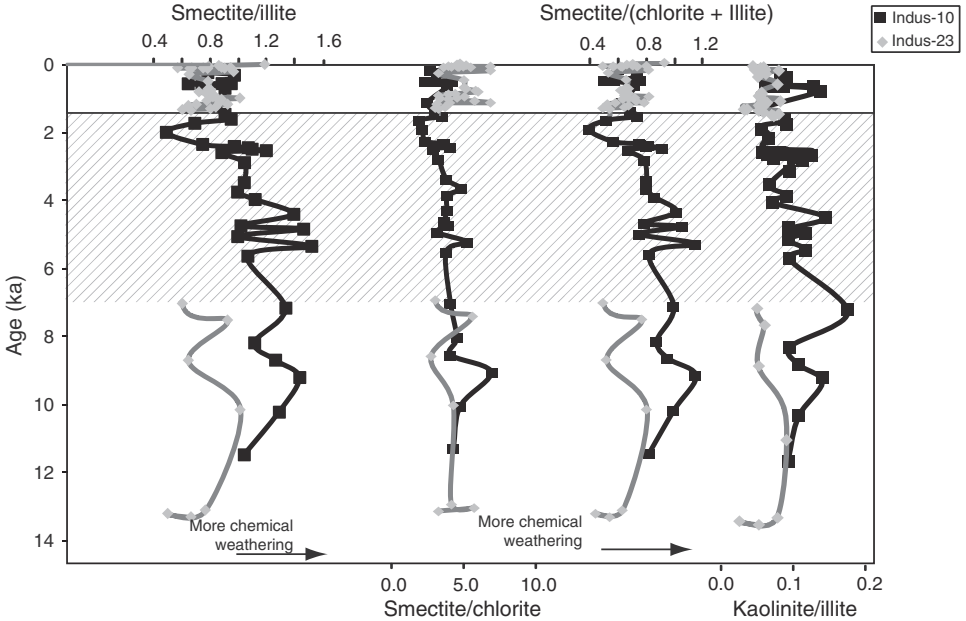

Fig. 7. Temporal variations in clay mineral ratios showing persistent decrease in smectite/illite values between 7 and 2 ka suggesting increasing in physical erosion at this time and less chemical weathering. Cross-shaded area indicates a hiatus at Indus-23.

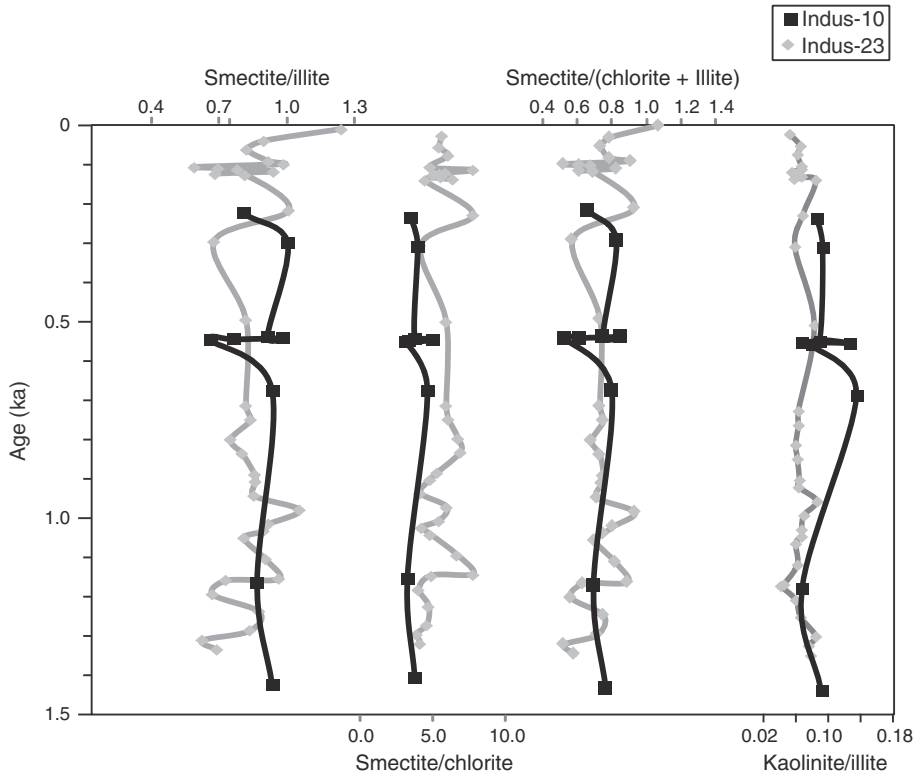

Fig. 8. Clay mineralogy variations for both Indus-10 and -23 since ~1.6 ka showing increasing, smectite/illite, smectite/(chlorite + illite), suggesting an increase in chemical weathering focused in the last 100–200 years.

Magnetic susceptibility decline sharply in Indus-23 between 10 ka and 8.5 ka during a period when the monsoon had reached maximum strength, as observed in the oxygen isotope records of Fleitmann et al. (2003). At Indus-10 however there is no such drop in magnetic susceptibility at this time, indeed the reverse is observed. If susceptibility tracks the flux of magnetite-bearing clastic flux to the ocean then its reduction at Indus-23 at a time when run-off might have increased is unexpected and suggests flux of sediment away from that site. Another possibility is that the magnetic mineralogy of the sediments at Indus-23 has been altered after deposition, possibly through diagenesis. Indus-10 behaves as might be expected in the context of a strengthening monsoon.

Both cores show an increase in FHWM (i.e. decreased illite crystallinity) during the Early Holocene indicating deposition of more weathered sediment at a time when the monsoon rains were strengthening. This is consistent with monsoonal moisture required for chemical weathering, although some of the weathered material being deposited might be reworked from older LGM-sediment driven by heavier monsoon rains.

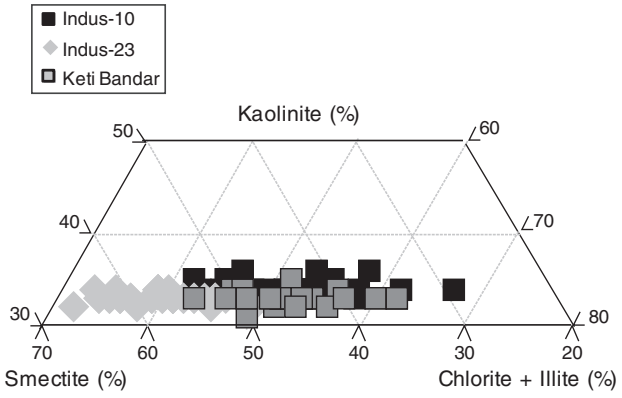

Fig. 9. Ternary plot showing variations in smectite, kaolinite, and chlorite + illite for Indus-10, Indus-23 and the Keti Bandar site. Indus-23 has systematically more smectite compared to the other two sites.

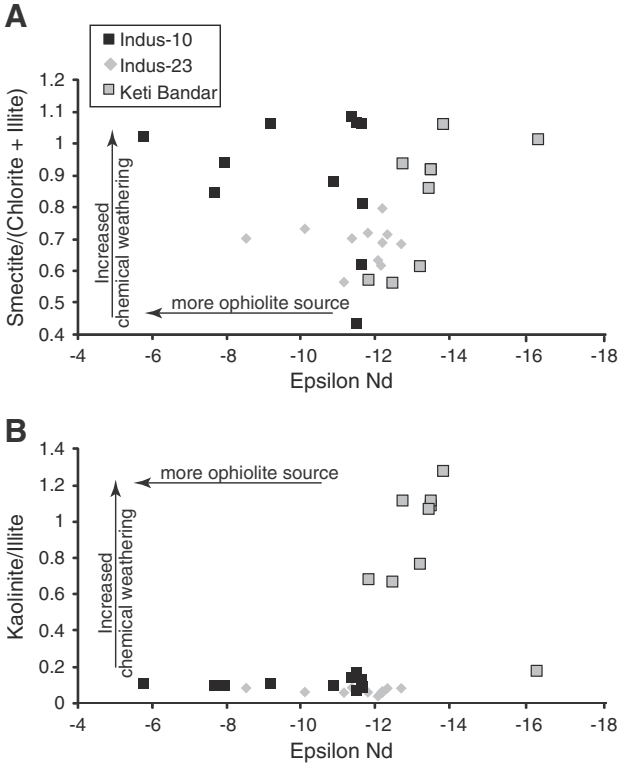

Fig. 10. Cross-plot between clay mineralogy and ε_{Nd} values in both the onshore and offshore environment (A) smectite/(chlorite + illite) and (B) kaolinite/illite. There is little correlation between any data from the three core sites.

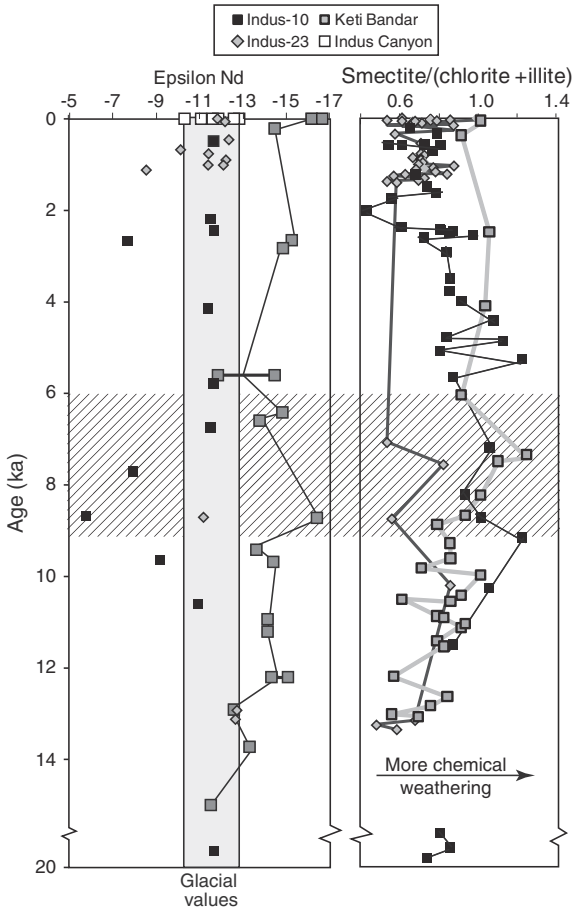

Fig. 11. Comparison of the offshore and onshore record of clay mineralogy and Nd isotopes, showing a slight correlation between variations in clay mineralogy and Nd at Indus-10 in the Early Holocene. Early Holocene increasing smectite/(chlorite + illite) ratios at Indus-10 could be linked to sediment supply from the Bela Ophiolite.

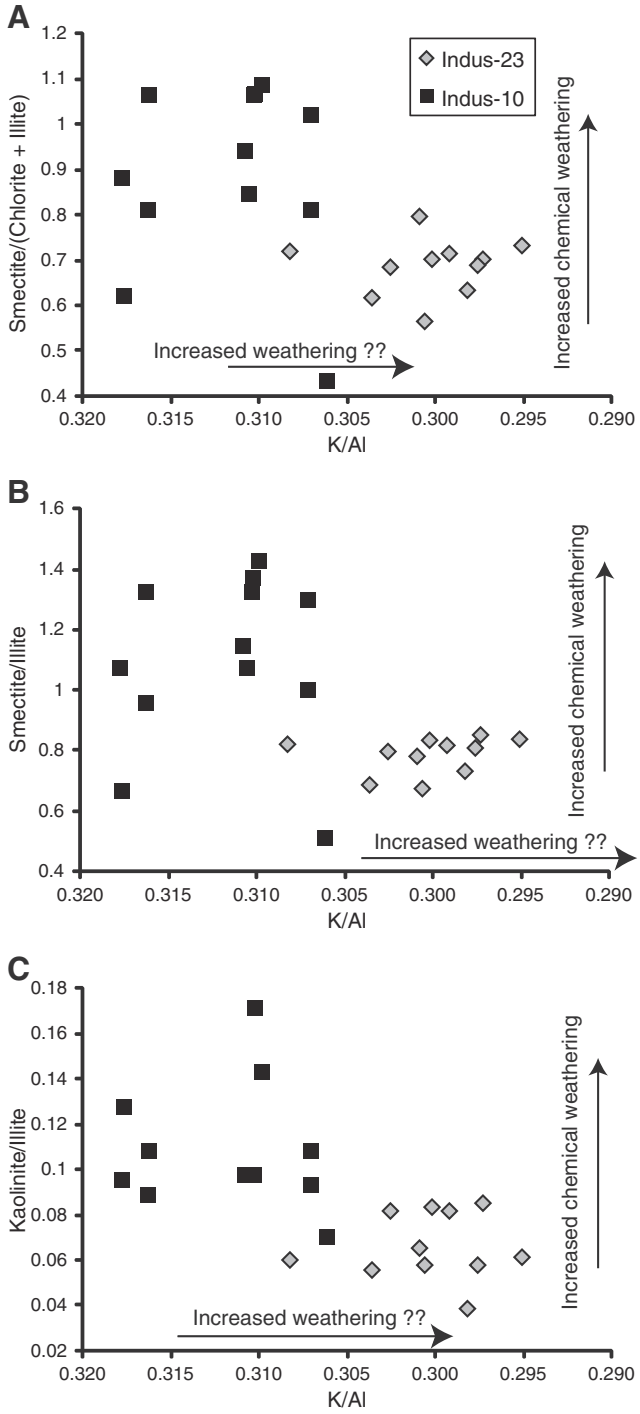

Fig. 12. Cross plots of clay mineral ratios against K/Al the most suitable geochemical weathering proxy for both Indus-10 and Indus-23 based on the observations of Limmer et al. (2012) (A) smectite/(chlorite + illite) (B) smectite/illite and (C) illite/kaolinite. The weak correlation between many of the clay-based weathering proxies and K/Al occurs because of the loss of potassium during very intense weathering, likely to occur if sediments are reworked.

4 ka is known to be a time of major climate change (Fleitmann et al., 2003; Gupta et al., 2003; Staubwasser and Weiss, 2006), which appears to have triggered a weathering response that is preserved in the sediment of Indus-10 (~560 cm core depth; Fig. 5). Magnetic susceptibility and smectite/(chlorite + illite) values drop as the monsoon weakened. It is this drought phase that has been correlated with the demise of the Indus-Harrapan civilization (Staubwasser et al., 2003; Madella and Fuller, 2006). Unfortunately the resolution of our records does not allow this climate event to be better resolved, although it is clear that it forms part of a long-term trend to weaker chemical weathering, as shown by increasing redness, higher hematite/goethite ratios and falling smectite/(chlorite + illite) values in Indus-10 between 8 and 2 ka. We conclude that clay mineralogy and DRS data can be correlated with palaeoclimatic data over periods >1000 years at Indus-10.

ε_{Nd} values indicate that some of the sediment deposited in the Early Holocene at Indus-10 was sourced from the Makran region, presumably through longshore drift, as well as from the Indus River mouth (Limmer et al., 2012). This transport could account for the higher smectite abundance at Indus-10 during the Early Holocene (Fig. 7), although the parallel trend seen at Keti Bandar instead suggests that there is a common climatic control to weathering in both the Makran and the main Indus basin. What is more surprising is the contrast between sediment from Indus-23 and the drill site at Keti Bandar, despite their relative proximity. Nonetheless, since 1.5 ka smectite/(illite + chlorite) values at the two sites are indistinguishable, suggesting that more recently all sediment west of the canyon is dominantly derived from the river mouth. During this time the monsoon is believed to have slightly strengthen, during what has been known as the Roman Warm Period (Chauhan et al., 2009), although there is no weathering response to this. The two sites only show moderate differences in magnetic susceptibility, redness and hematite/goethite since 2 ka.

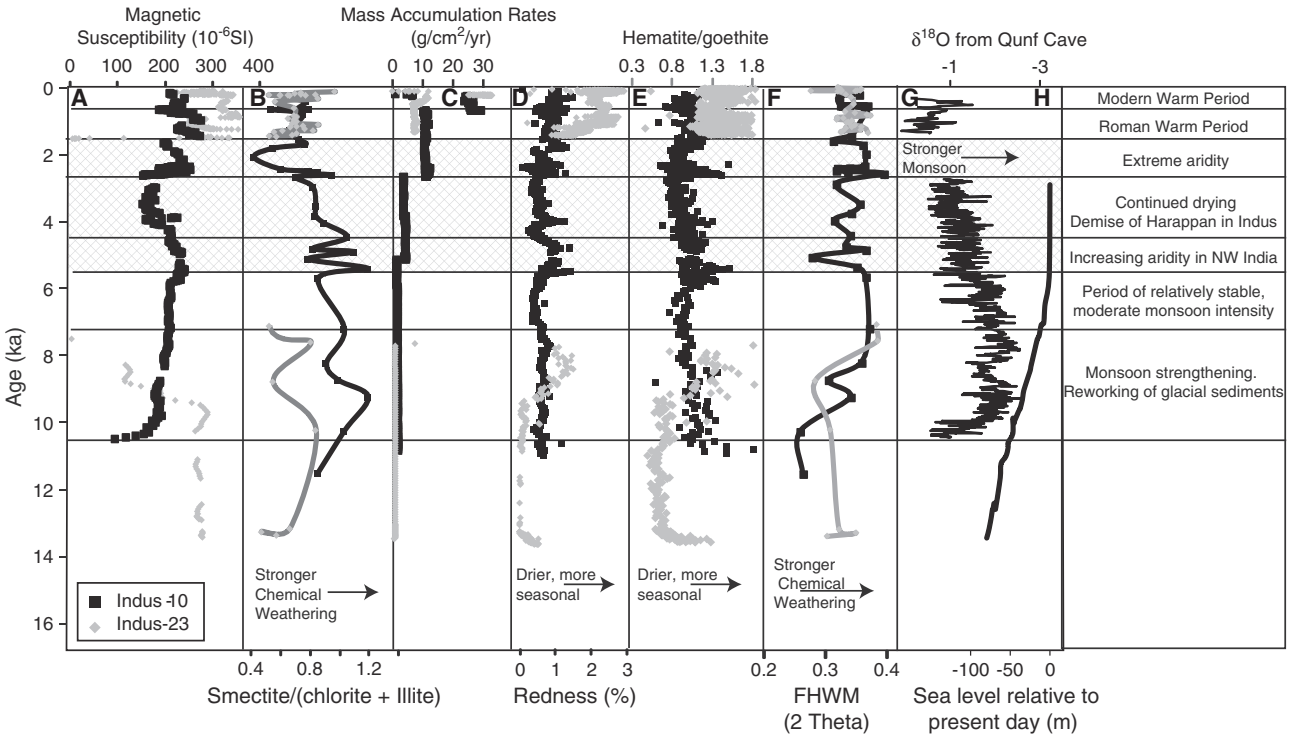

Fig. 13. Temporal variations of physical properties compared to regional climate and sea level records since 16 ka. (A) Magnetic susceptibility, (B) smectite/(chlorite + illite), (C) mass accumulation rates, (D) redness, (E) hematite/goethite, (F) illite crystallinity FHWM, (G) ^{18}O from Qunf Cave (Fleitmann et al., 2003), and (H) sea level reconstruction of Bard et al. (1996). Cross shaded area indicates period of weakening and weak summer monsoon rains.

Mass accumulation rates (MAR) increased at Indus-10 during the Holocene. Although rising sea level created accommodation space on the shelf this process was completed by ~6 ka, before the increasing MAR as noted. The hiatus in the section at Indus-23 makes it impossible to derive a meaningful long-term MAR reconstruction. We have no way of knowing if the higher rates at Indus-10 are just a local anomaly or if sediment delivery rates really increased across the shelf. MAR increased at both sites after ~2 ka and particularly since 500 years ago when there is a modest increase in summer monsoon intensity (von Rad et al., 2002; Fleitmann et al., 2003). However, this increase is out of proportion to the modest climate change and more likely indicates anthropogenic activity, such as cultivation or irrigation of the floodplain, which is widely linked to enhanced erosion and sediment delivery to deltas worldwide (Syvitski et al., 2005).

6. Conclusions

A study of the geophysical properties and clay mineralogy of sediments from the Indus Shelf was conducted at two sites in ~70 m water depths west of the Indus River mouth and canyon. Changing clay mineralogy reflects a climatically driven evolution in chemical weathering in the onshore basin. The coherent variation in smectite/(illite + chlorite) and illite crystallinity with monsoon intensity at Indus-10 is consistent with a climatic control to chemical weathering processes since 14 ka. However, we do not know if this is a direct response to stronger summer monsoon rains, or stronger reworking of pre-existing, more weathered material. Increasing hematite/goethite in the Early Holocene indicates that reworking for older LGM sediment was important at least at Indus 23. Hematite/goethite values show a gradual fall at Indus-10 from 11 to 2 ka, suggestive of reduced seasonality as the summer monsoon weakened. At Indus-10 susceptibility has increased first rapidly after 10.5 ka, and then steadily after 8 ka until 5.5 ka, mostly during a period of strong summer monsoon. Falling susceptibility of the 5.5 ka correlates with the weaker monsoon, although increases after 2.5 ka are hard to relate to climate records. Sedimentation rates gradually increased during the Holocene, most notably in the last 200 years, which is attributed to anthropogenic modification of the floodplain, boosting sediment delivered to the ocean, as a result of reworking of older weathered materials. Strengthening of the monsoon during this recent period has been minor and is unlikely to be the trigger of the trend since ~2 ka. We conclude that there are links between climatic variation and clay mineralogy on the Indus Shelf, but that reworking can make this hard to relate to weathering processes in the Indus flood plains at all locations. The most promising weathering proxies are smectite/(illite + chlorite) and illite crystallinity, but it is unclear whether the positive correlation between weathering intensity and summer monsoon strength is driven by direct response, or more by erosion and reworking of material weathered during earlier time periods.

Acknowledgements

The work was funded by a NERC studentship grant NE/G002029/1 for DL. The work was also supported by a grant from the International Association of Sedimentologists (IAS) for clay mineral analysis and a NERC facility grant for additional radiocarbon dates (NRCF allocation 1529.0311). We thank Christophe Colin and Nathalie Fagel for their constructive reviews. DL thanks Guy Rothwell and Suzanne MacLachlan at BOSCORF for training on the Geotek MSCL-XYZ and technical assistance and Jeremy Sothcott for his help in preparing cores for bulk density measurements. Anwar Alizai and Raja Ganeshram are thanked for useful discussions. DL also thanks Ian Philips for his assistance with the XRD analysis. DL and CK thank Nicola Pressling for the use of the Barrington MS2 Magnetic Susceptibility metre. PC thanks the Hanse Wissenschaftskolleg, Germany for the time to think about monsoon river and delta systems.

References

Abrajevitch, A., Van der Voo, R., Rea, D.K., 2009. Variations in relative abundances of goethite and hematite in Bengal Fan sediments: climate vs diagenetic signals. Marine Geology 267, 191–206.

Adler, R.E., Polyak, L., Ortiz, J.D., Kaufman, D.S., Channel, J.E.T., Xuan, C., Grottoli, A.G., Sellen, E., Crawford, K.A., 2009. Sediment record from the western Artic Ocean with an improved Late Quaternary age resolution: HOTRAX core HLY0503-8JPC. Global and Planetary Change 68, 18–29.

Alizai, A., Hillier, S., Clift, P.D., Giosan, L., 2012. Clay mineral variations in Holocene terrestrial sediments from the Indus Basin; a response to SW Asian Monsoon variability. Quaternary Research, http://dx.doi.org/10.1016/j.yqres.2012.01.008.

Almogi-Labin, Bar-Matthews, M., Shriki, D., Kolosovosky, E., Paterne, M., Schillman, B., Ayalon, A., Aizenshtat, Z. And, Matthews, A., 2009. Climatic Variability during the last ~90 ka of the southern and northern Levante Basin as evident from marine records and speleotherms. Quaternary Science Reviews 28, 2882–2896.

An, Z., Kutzbach, J.E., Prell, W., Porter, S.C., 2001. Evolution of Asian monsoons and phased uplift of the Himalaya–Tibetan plateau since Late Miocene times. Nature 411, 62–66.

Balsam, W.L., Otto-Bliesner, B.L., Deaton, B.C., 1995. Modern and last glacial maximum Aeolian sedimentation patterns in the Atlantic Ocean interpreted from sediment iron oxide content. Paleoceanography 10, 493–507.

Balsam, W.L., Damuth, J.E., Deaton, B., 1999. Evaluate optical lightness as a proxy for carbonate content in marine cores. Marine Geology 161, 141–153.

Balsam, W.L., Damuth, J.E., 2000. Further Investigations of shipboard vs shore-based spectral data: implications for interpreting leg 164 sediment composition. In: Paul, C.K., Matsumoto, R., Wallace, P.J., Dillion, W.P. (Eds.), Science Results Proceedings of ODP scientific results, Volume 164, pp. 313–324.

Bard, E., Hamelin, B., Arnold, M., Montaggioni, L.F., Cabioch, G., Faure, G., Rougerie, F., 1996. Deglacial sea-level record from Tahiti corals and the timing of global meltwater discharge. Nature 382, 241–244.

Biscaye, P.E., 1965. Mineralogy and sedimentation of Recent deep-sea clay in the Atlantic Ocean and adjacent seas and oceans. Geological Society of America Bulletin 76, 803–832.

Blaxland, A.B., 1974. Geochemistry and geochronology of chemical weathering, Butler Hill Granite, Missouri. Geochimica et Cosmochimica Acta 38 (6), 843–852.

Boulay, S., Colin, C., Trentesaux, A., Pluquet, F., Bertaux, J., Blamart, D., Buehring, C., Wang, P., 2003. Mineralogy and sedimentology of Pleistocene sediment in the South China Sea (ODP Site 1144). Proceedings of the Ocean Drilling Program, Scientific Results 184, 1–21.

Boulay, S., Colin, C., Trentesaux, Frank, N., Liu, Z., 2005. Sediment sources and East Asian Monsoon intensity over the last 450 ky. Mineralogical and geochemical investigations on South China Sea sediments. Palaeogeography, Palaeoclimatology, Palaeoecology 228, 260–277.

Bouquillon, A., Chamley, H., Frolich, F., 1989. Sedimentation argileuse au Cenozoique del'Ocean Indien Nord Oriental. Oceanologica Acta 12, 133–147.

Campbell, I.B., Claridge, G., 1982. The influence of moisture on the development of soils of the cold deserts of Antarctica. Geoderma 28, 221–228.

Chamley, H., 1989. Clay Sedimentology. Springer-Verlag, Berlin.

Chamley, H., 2001. Clay Mineralogy. In: Steele, J.H., Thorpe, S.A., Turekian, K.K. (Eds.), Encyclopaedia of Ocean Sciences, pp. 462–471.

Chauhan, O.S., Vogelsang, E., Basavaiah, N., Kader, U.S.A., 2009. Reconstruction of the southwest monsoon during the last 3 ka, from the continental margin of the southeastern Arabian Sea. Journal of Quaternary Science 25, 798–807.

Clift, P.D., Blusztajn, J.S., 2005. Reorganization of the western Himalayan river system after five million years ago. Nature 438 (7070), 1001–1003.

Clift, P.D., Shimizu, N., Layne, G., Gaedicke, C., Schlüter, H.U., Clark, M., Amjad, S., 2001. Development of the Indus Fan and its significance for the erosional history of the western Himalaya and Karakoram. Geological Society of America Bulletin 113, 1039–1051.

Clift, P., Lee, J.I., Clark, M.K., Blusztajn, J., 2002. Erosional response of south China to arc rifting and monsoonal strengthening; a record from the South China Sea. Marine Geology 184, 207–226.

Clift, P.D., Campbell, I.H., Pringle, M.S., Carter, A., Zhang, X., Hodges, K.V., Khan, A.A., Allen, C.M., 2004. Thermochronology of the modern Indus River bedload; new insight into the control on the marine stratigraphic record. Tectonics 23 (TC5013).

Clift, P.D., Giosan, L., Blusztajn, J., Campbell, I.H., Allen, C., Pringle, M., Tabrez, A.R., Danish, M., Rabbani, M.M., Alizai, A., Carter, A., Lückge, A., 2008. Holocene erosion of the lesser Himalaya triggered by intensified summer monsoon. Geology 36, 79–82.

Colin, C., Turpin, L., Bertaux, J., Desprairies, A., Kissel, C., 1999. Erosional history of the Himalayan and Burman ranges during the last two interglacial cycles. Earth and Planetary Science Letters 171, 647–660.

Colin, C., Turpin, L., Blamart, D., Frank, N., Kissel, C., Duchamp, S., 2006. Evolution of weathering patterns in the Indo-Burman Ranges over the last 280kyr: effects of sediment provenance on $^{87}Sr/^{86}Sr$ ratios tracer. Geochemistry, Geophysics, Geosystems 7 (3), Q03007.

Colin, C., Siani, G., Sicre, M.-A., Liu, Z., 2010. Impact of the East Asian monsoon rainfall changes on the erosion of the Mekong River basin over the past 25,000 yr. Marine Geology 271, 84–92.

Croft, D.J., Pye, K., 2004. Colour theory and the evaluation of an instrumental method of measurement using geological samples for forensic applications. In: Pye, K., Croft, D.J. (Eds.), Forensic Geoscience: Principles, Techniques and Applications: Geological Society, London, Special publications, 232, pp. 49–62.

De Visser, J.P., Chamley, H., 1990. Clay mineralogy of the Pliocene and Pleistocene of Hole 653A, Western Tyrrhenian Sea (ODP leg 107). Proceedings of the Ocean Drilling Program Scientific Results 107, 323–332.

Debrabant, P., Fagel, N., Chamley, H., Bout, V., Caulet, J.-P., 1993. Neogene to Quaternary clay fluxes to the Central Indian basin. Palaeogeography, Palaeoclimatology, Palaeoecology 103, 117–131.

Debret, M., Desmet, M., Balsam, W., Copard, Y., Francus, P., Laj, C., 2006. Spectrophotometer analysis of Holocene sediments from an anoxic fjord: Saanich Inlet, British Columbia, Canada. Marine Geology 229, 15–28.

Debret, M., Sebag, D., Desmet, M., Balsam, W., Copard, Y., Mourier, B., Susperrigui, A.-S., Arnaud, F., Bentaleb, I., Chapron, E., Lallier-Vergès, E., Winiarski, T., 2011. Spectrocolorimetric interpretation of sedimentary dynamics: the new "Q7/4 diagram". Earth-Science Reviews 109, 1–19.

DeMenocal, P., Bloemendal, J. And, King, J., 1991. A rock magnetic record of monsoonal dust deposition to the Arabian Sea: evidence for a shift in the mode of deposition at 2.4 Ma. Proceedings of the Ocean Drilling Program Scientific Results 117, 389–407.

Enzel, Y., Ely, L.L., Mishra, S., Ramesh, R., Amit, R., Lazar, B., Rajaguru, S.N., Baker, V.R., Sandle, A., 1999. High-resolution Holocene environmental changes in the Thar Desert, northwestern India. Science 284, 125–128.

Fagel, N., 2007. Clay minerals, deep circulation, and climate marine clay minerals, deep circulation and climate. In: Hillaire-Marcel, C., de Vernal, A. (Eds.), Paleoceanography of the Late Cenozoic. : Methods, Volume 1. Elsevier, Amsterdam, pp. 139–184.

Fagel, N., Debrabant, P., Andre, L., 1994. Clay supplies in the Central Indian Basin since the Late Miocene: climatic or tectonic control? Marine Geology 122, 151–172.

Fleitmann, D., Burns, S.J., Mudelsee, M., Neff, U., Kramers, J., Mangini, A., Matter, A., 2003. Holocene forcing of the Indian monsoon recorded in a stalagmite from southern Oman. Science 300, 1737–1739.

Garzanti, E., Vezzoli, G., Ando, S., Paparella, P., Clift, P.D., 2005. Petrology of Indus River sands: a key to interpret erosion history of the Western Himalayan Syntaxis. Earth and Planetary Science Letters 229, 287–302.

Giosan, L., Constantinescu, S., Clift, P.D., Tabrez, A.R., Danesh, M., Inam, A., 2006. Recent morphodynamics of the Indus shore and shelf. Continental Shelf Research 26, 1668–1684.

Goldstein, S.L., O'Nions, R.K., Hamilton, P.J., 1984. A Sm–Nd isotopic study of atmospheric dusts and particulates from major river systems. Earth and Planetary Science Letters 70, 221–236.

Gupta, A.K., Anderson, D.M., Overpeck, J.T., 2003. Abrupt changes in the Asian southwest monsoon during the Holocene and their links to the North Atlantic Ocean. Nature 421, 354–357.

Gupta, A.K., Das, M.A., Anderson, D.M., 2005. Solar influence on the Indian summer monsoon during the Holocene. Geophysical Research Letters 32, L17703.

Helmke, J.P., Schulz, M. And, Bauch, H.A., 2002. Sediment-color record from the Northeast Atlantic reveals patterns of millenial-scale climate variability during the past 500,000 years. Quaternary Research 57, 49–57.

Hillier, S., 1995. Erosion, sedimentation and sedimentary origin of clays. In: Velde, B. (Ed.), Origin and Mineralogy of Clays: Clays and the Environment, pp. 162–219.

Hillier, S., 2003. Quantitative analysis of clay and other minerals in sandstones by X-ray powder diffraction (XRPD). In: Worden, R.H., Moorad, S. (Eds.), Clay mineral cements in sandstones: International Association of Sedimentologists Special Publications, Vol. 34, pp. 213–251.

Hughen, K.A., Baillie, M.G.L., Bard, E., Bayliss, A., Beck, J.W., Bertrand, C., Blackwell, P.G., Buck, C.E., Burr, G., Cutler, K.B., Damon, P.E., Edwards, R.L., Fairbanks, R.G., Friedrich, M., Guilderson, T.P., Kromer, B., McCormac, F.G., Manning, S., Ramsey, C.B., Reimer, P.J., Reimer, R.W., Remmele, S., Southon, J.R., Stuvier, M., Talamo, S., Taylor, F.W., van der Plicht, J., Weyhenmeyer, C.W., 2009. Marine 04 radiocarbon calibration curves 0–50,000 years cal BP. Radiocarbon 46, 1059–1086.

Inam, A., Clift, P.D., Giosan, L., Tabrez, A.R., Tahir, M., Rabbani, M.M., Danish, M., 2007. The geographic, geological and oceanographic setting of the Indus River. In: Gupta, A. (Ed.), Large Rivers: Geomorphology and Management. John Wiley and Sons, pp. 333–345.

Jarrard, R.D., Vanden Berg, M.D., 2006. Sediment mineralogy based on visible and near-infrared reflectance spectroscopy. In: Rothwell, R.G. (Ed.), New techniques in sediment core analysis: Geological Society, London Special Publication, 267, pp. 129–140.

Ji, J., Shen, J., Balsam, W., Chen, J., Liu, L., Liu, X., 2005. Asian monsoon oscillations in the northeast Qinghai–Tibet Plateau since the last glacial as interpreted from visible reflectance of Qinghai Lake sediments. Earth and Planetary Science Letters 233, 61–70.

Kisch, H.J., 1983. Mineralogy and petrology of burial diagenesis (burial metamorphism) and incipient metamorphism in clastic rocks. In: Larsen, G., Chilingar, G.V. (Eds.), Diagenesis and Sediments and Sedimentary Rocks. Elsevier, Amsterdam, pp. 289–493.

Kolla, V., Kostecki, J.A., Robinson, F., Biscaye, P.E., Ray, P.K., 1981. Distributions and origins of clay minerals and quartz in surface sediments of the Arabian Sea. Journal of Sedimentary Petrology 51, 563–569.

Kübler, B., Jaboyedoff, M., 2000. Illite crystallinity: concise review paper Comptes Rendus de l'Academie des Sciences-Series IIA. Earth and Planetary Science 331, 75–89.

Kumar, A.A., Rao, V.P., Patil, S.K., Kessarkar, P.M., Thambam, M., 2005. Rock magnetic records of the sediments of the eastern Arabian Sea: evidence for Late Quaternary climate change. Marine Geology 220, 59–82.

Lamy, F., Hebbeln, D., Wefer, G., 1998. Late Quaternary precessional cycles of terrigenous sediment input off the Norte Chico, Chile (27.5°S) and palaeoclimatic implications. Palaeogeography, Palaeoclimatology, Palaeoecology 141, 233–251.

Limmer, D.R., Böning, P., Giosan, L., Ponton, C., Köhler, C.M., Cooper, M.J., Tabrez, A.R., Clift, P.D., 2012. Geochemical record of Holocene to Recent sedimentation on the Western Indus Shelf, Arabian Sea. Geochemistry, Geophysics, Geosystems 13 (1), Q01008.

Liu, Z., Trentesaux, A., Clemens, S.C., Colin, C., Wang, P., Huang, B., Boulay, S., 2003. Clay mineral assemblages in the northern South China Sea: implications for East Asian Monsoon evolution over the past 2 million years. Marine Geology 201, 133–146.
Liu, X., Dong, H., Yang, X., Herzschuh, U., Zhang, E., Stuut, J.-B.W., Wang, Y., 2009. Late Holocene forcing of the Asian winter and summer as evidenced by proxy records from the northern Qinghai–Tibetan plateau. Earth and Planetary Science Letters 280, 276–284.
Madella, M., Fuller, D.Q., 2006. Palaeoecology and the Harappan Civilization of South Asia: a reconsideration. Quaternary Science Reviews 25, 1283–1301.
McNichol, A.P., Gagnon, A.R., Osborne, E.A., Hutton, D.L., VonReden, K.F., Schneider, R.J., 1995. Improvements in procedural blanks at NOSAMS: reflections of improvements in sample preparation and accelerator operation. Radiocarbon 37, 683–691.
Milliman, J.D., Quiraishee, G.S., Beg, M.A.A., 1984. Sediment discharge from the Indus River to the Ocean: past, present future. In: Haq, B.U., Milliman, J.D. (Eds.), Marine Geology and Oceanography of Arabian Sea and Coastal Pakistan Von Nostrand and Reinhold Company, pp. 65–70.
Moore, D.M., Reynolds, R.C., 1989. X-Ray Diffraction and the Identification of Clay Minerals. Oxford University Press.
Naidu, P.D., 2006. Link between Western Arabian sea surface temperature and Summer Monsoon strength and high latitude abrupt climate events. Journal of the Geological Society of India 68, 379–385.
Nederbragt, A.J., Dunbar, R.B., Osborn, A.T., Palmer, A., Thurow, J.W., Wagner, T., 2006. Sediment colour analysis from digital images and correlation with sediment composition. In: Rothwell, R.G. (Ed.), New techniques in sediment core analysis: Geological Society, London Special Publication, 267, pp. 113–128.
Nesbitt, H.W., Fedo, C.M., Young, G.M., 1997. Quartz and feldspar stability, steady and non-steady-state weathering, and petrogenesis of siliciclastic sands and muds. Journal of Geology 105 (2), 173–191.
Pandarinath, K., 2009. Clay minerals in SW Indian Continental Shelf sediment cores as indicators of provenance and palaeomonsoon conditions: a statistical approach. International Geology Review 51, 145–165.
Papavassiliou, C.T., Cosgrove, M.E., 1982. The geochemistry of DSDP sediments from Site 223, Indian Ocean. Chemical Geology 37, 299–315.
Possehl, G.L., 1999. Indus Age. The Beginnings. University of Pennsylvania Press, Philadelphia.
Prins, M.A., Postma, G., Cleveringa, J., Cramp, A., Kenyon, N.H., 2000. Controls on terrigenous sediment supply to the Arabian Sea during the late Quaternary: the Indus Fan. Marine Geology 169, 327–349.
Rao, V.P., Rao, B.R., 1995. Provenance and distribution of clay minerals in the sediments of the western continental shelf and slope of India. Continental Shelf Research 15, 1757–1771.
Reimer, P.J., Baillie, M.G.L., Bard, E., Bayliss, A., Beck, J.W., Blackwell, P.G., Bronk Ramsey, C., Buck, C.E., Burr, G.S., Edwards, R.L., Friedrich, M., Grootes, P.M., Guilderson, T.P., Hajdas, I., Heaton, T.J., Hogg, A.G., Hughen, K.A., Kaiser, K.F., Kromer, B., McCormac, F.G., Manning, S.W., Reimer, R.W., Richards, D.A., Southon, J.R., Talamo, S., Turney, C.S.M., van der Plicht, J., Weyhenmeyer, C.E., 2009. IntCal09 and Marine09 radiocarbon age calibration curves, 0–50,000 years cal BP. Radiocarbon 51, 1111–1150.
Roberts, A.P., Lewin-Harris, J.C., 2000. Marine magnetic anomalies: evidence that 'tiny wiggles' represent short-period geomagnetic polarity intervals. Earth and Planetary Science Letters 183, 375–388.
Rodgers, J., Thobobeaux, D., Cui, X., Martin, V., Watson, M., Knowlton, J., 2008. Textile technology instrumental and operational impacts on Spectrophotometer Color Measurements. Journal of Cotton Science 12, 287–297.
Rogerson, M., Weaver, P.E.E., Rohling, E.J., Lourens, L.J., Murray, J.W., Hayes, A.J., 2006. Colour logging as a tool in high resolution palaeoceanography. In: Rothwell, R.G. (Ed.), New techniques in sediment core analysis: Geological Society, London Special Publication, 267, pp. 99–112.
Sarkar, A., Ramesh, R., Somayajulu, B.I.K., Agnihotri, R., Jul, A.J.T., Burr, G.S., 2000. High resolution Holocene monsoon record from the eastern Arabian Sea. Earth and Planetary Science Letters 177, 209–218.
Schwertmann, U., 1971. Transformation of hematite–goethite in soils. Nature 232, 624–625.
Sirocko, F., Lange, H., 1991. Clay mineral accumulation rates in the Arabian Sea during the Late Quaternary. Marine Geology 97, 105–119.
Sirocko, F., Garbe-Schönberg, D., Devey, C., 2000. Processes controlling trace element geochemistry of Arabian Sea sediments during the past 25,000 years. Global and Planetary Change 26, 217–303.
Staubwasser, M., Sirocko, F., 2001. On the formation of laminated sediments on the continental margin of Pakistan: the effects of sediment provenance and sediment redistribution. Marine Geology 172, 43–56.
Staubwasser, M., Weiss, H., 2006. Holocene climate and cultural evolution in late prehistoric-early historic West Asia. Quaternary Research 66, 372–387.
Staubwasser, M., Sirocko, F., Grootes, P.M., Erlenkeuser, H., 2002. South Asian Monsoon climate and radiocarbon in the Arabian Sea during the early and middle Holocene. Paleoceanography 17 (4), 1063.
Staubwasser, M., Sirocko, F., Grootes, P.M., Segl, M., 2003. Climate change at the 4.2 ka BP termination of the Indus valley civilisation and Holocene south Asia monsoon variability. Geophysical Research Letters 30, 1425–1428.
St-Onge, G., Mulder, T., Francus, P., Long, B., 2007. Chapter two: continuous properties of cored marine sediments. In: Hillaire, C., Anthony, E.J. (Eds.), Proxies in Late Cenozoic Paleoceanography. University of Quebec, Montreal, pp. 63–98.
Suczek, C.A., Ingersoll, R.V., 1985. Petrology and Provenance of Cenozoic sand from the Indus cone and the Arabian Basin, DSDP sites 221,222 and 224. Journal of Sedimentary Petrology 55, 340–346.
Sun, Y., Chen, T., Xie, Q., 2009. Magnetic susceptibility of the Xifeng Section and its palaeoclimatic significance. Chinese Journal of Geochemistry 28, 81–85.
Syvitski, J.P.M., Vörösmarty, C.J., Kettner, A.J., Green, P., 2005. Impact of humans on the flux of terrestrial sediment to the global coastal ocean. Science 308, 376–380.
Thamban, M., Rao, V.P., Schneider, R.R., 2002. Reconstruction of late Quaternary monsoon oscillations based on clay mineral proxies using sediment cores from the western margin of India. Marine Geology 186, 527–539.
Thamban, M., Naik, S.S., Mohan, R., Rajakumar, A., Basavaiah, N., D'Souza, W., Kerkar, S., Subramaniam, M.M., Sudahkar, M., Pandey, P.C., 2005. Changes in the source and transport mechanism of terrigenous input to the Indian Sector of the Southern Ocean during the Late Quaternary and its palaeoceanographic implications. Journal of Earth System Science 114, 443–452.
Thiry, M., 2000. Palaeoclimatic interpretation of clay minerals in marine deposits: an outlook from the continental origin. Earth-Science Reviews 49, 201–221.
von Rad, U., Ali Khan, A., Berger, W.H., Rammlmair, D., Treppke, U., 2002. Varves, turbidites and cycles in the upper Holocene sediments (Makran slope, northern Arabian Sea). In: Clift, P.D., Kroon, D., Gaedicke, C., Craig, J. (Eds.), The Tectonic and Climatic Evolution of the Arabian Sea Region: Geological Society Special Publication, 195, pp. 387–406.
Wan, S., Li, A., Clift, P.D., Stuut, J.-B.W., 2007. Development of the East Asian monsoon: mineralogical and sedimentologic records in the northern South China Sea since 20 Ma. Palaeogeography, Palaeoclimatology, Palaeoecology 254 (3–4), 561–582.
Wilson, M.J., 1999. The origin and formation of clay minerals in soils: past, present and future perspectives. Clay Minerals 34, 7–25.
Yancheva, G., Nowaczyk, N.R., Mingram, J., Dulski, P., Schettler, G., Negendank, J.F.W., Liu, J., Sigman, D.M., Peterson, L.C., Haug, G.H., 2007. Influence of the intertropical convergence zone on the East Asian Monsoon. Nature 445, 74–77.
Zang, Y.E., Ji, J., Balsam, W.L., Liu, L., Chen, J., 2007. High resolution hematite and goethite records from ODP 1143, South China Sea: Co evolution of monsoonal precipitation and El Nino over the past 600,000 years. Earth and Planetary Science Letters 264, 136–150.